

# Biomedical Materials



## PAPER


# Bioactive snail mucus-slime extract loaded chitosan scaffolds for hard tissue regeneration: the effect of mucoadhesive and antibacterial extracts on physical characteristics and bioactivity of chitosan matrix

RECEIVED  
26 March 2021

REVISED  
26 August 2021

ACCEPTED FOR PUBLICATION  
2 September 2021

PUBLISHED  
22 September 2021

Merve Perpelek<sup>1</sup>, Sedef Tamburaci<sup>2</sup>, Selma Aydemir<sup>3</sup>, Funda Tihminlioglu<sup>2,\*</sup> , Basak Baykara<sup>3</sup>, Ahmet Karakasli<sup>4</sup> and Hasan Havitcioglu<sup>4</sup>

<sup>1</sup> Biomechanics Graduate Program, Dokuz Eylul University, Izmir, Turkey

<sup>2</sup> Department of Chemical Engineering, Izmir Institute of Technology, Gulbahce Campus, Urla, Izmir, Turkey

<sup>3</sup> Department of Histology and Embryology, Dokuz Eylul University, Izmir, Turkey

<sup>4</sup> Department of Orthopedics and Traumatology, Dokuz Eylul University, Izmir, Turkey

\* Author to whom any correspondence should be addressed.

E-mail: [fundatihminlioglu@iyte.edu.tr](mailto:fundatihminlioglu@iyte.edu.tr)

**Keywords:** *Helix aspersa*, mucus, slime, chitosan, scaffold, bone, cartilage

## Abstract

Biobased extracts comprise various bioactive components and they are widely used in tissue engineering applications to increase bioactivity as well as physical characteristics of biomaterials. Among animal sources, garden snail *Helix aspersa* has come into prominence with its antibacterial and regenerative extracts and show potential in tissue regeneration. Thus, in this study, bioactive *H. aspersa* extracts (slime, mucus) were loaded in chitosan (CHI) matrix to fabricate porous scaffolds for hard tissue regeneration. Physical, chemical properties, antimicrobial activity was determined as well as *in vitro* bioactivity for bone and cartilage regeneration. Mucus and slime incorporation enhanced mechanical properties and biodegradation rate of CHI matrix. Scanning electron microscopy images showed that the average pore size of the scaffolds decreased with higher extract content. Mucus and slime extracts showed antimicrobial effect on two bacterial strains. *In vitro* cytotoxicity, osteogenic and chondrogenic activity of the scaffolds were evaluated with Saos-2 and SW1353 cell lines in terms of Alkaline phosphatase activity, biomineralization, GAG, COMP and hydroxyproline content. Cell viability results showed that extracts had a proliferative effect on Saos-2 and SW1353 cells when compared to the control group. Mucus and slime extract loading increased osteogenic and chondrogenic activity. Thus, the bioactive extract loaded CHI scaffolds showed potential for bone and cartilage regeneration with enhanced physical properties and *in vitro* bioactivity.

## 1. Introduction

Bone and cartilage damage is a highly observed clinical situation in orthopedic field. Although there are traditional treatments known as auto-grafting and allografting techniques, they have risk factors such as donor site morbidity, infections and immunogenic reactions [1, 2]. In the conventional hard tissue-engineering paradigm, combinations of cells and bioactive molecules are seeded on three-dimensional biomaterial scaffolds to create an implantable 'osteogenic' and 'chondrogenic' implant [3]. When designing a scaffold, the main aim is to

achieve the ideal structure in which cells can survive, proliferate and differentiate into specific tissues and can replace the natural extracellular matrix structure [4]. Scaffolds should be appropriately similar with the target tissue by consisting of bioactive components compatible with the body, providing physical properties as suitable degradation rate, and mechanical strength. It should also have a porous structure that allows cell attachment, allowing oxygen and nutrient diffusion.

Many polymers have been extensively investigated as biomaterials for bone and cartilage regeneration. These biomaterials include synthetic or natural

polymers such as polycaprolactone, poly (lactic-co-glycolic acid), poly (ethylene glycol), poly (vinyl alcohol), polyurethane, alginate, gelatin, collagen and chitosan (CHI). Recently, naturally derived biopolymers have been identified as potential biomaterials to with their several advantages over synthetic polymers as higher biocompatibility, biodegradability and remodeling. Therefore, biopolymers have ability to adequately support and induce cell adhesion, migration, proliferation and differentiation. In particular, when implanted into a defective area, naturally derived biomaterials can enhance the cell attachment and migration from the surrounding environment due to their similar structure with the target tissue. Therefore, they induce extracellular matrix formation and promote tissue repair [5]. On the other hand, natural polymers often show poor mechanical properties [6]. In this context, CHI is widely used biopolymer in hard tissue engineering due to its biocompatibility, biodegradability, non-toxic effect, antibacterial properties and similarity to some glycosaminoglycan (GAG) structures in the extracellular matrix. Currently bioactive agents are used as reinforcement in biopolymers. To mimic composite structure of hard tissue and overcome their limitations. Thus, composite structure can provide stability and enhance the mechanical properties as well as inducing bioactivity. Medicinal plants, animal extracts and their bioactive compounds have been incorporated in polymers to be used in hard tissue regeneration to improve attachment, proliferation, and differentiation of bone and cartilage cells. The extracts of medicinal plants such as *Cissus quadrangularis*, *Withania somnifera*, *Tinospora cordifolia*, *Urtiga dioica* and *Gum Arabic* have been observed to increase bone cell viability and promote the proliferation of cells [7–10].

Among animal extracts, different snail species secretions have been investigated as bioactive agents for especially skin tissue regeneration. It was found that snail secretion induces fibroblast proliferation [11, 12], enhances wound healing by increasing tissue formation, reducing pain [13] and shows antimicrobial activity against many types of bacteria [14–16]. Recent studies have revealed that *Helix aspersa*, generally known as garden snail, has two types of secretions as mucus and slime. Snail secretions have many components such as allantoin, collagen, elastin, glycolic acid, GAG, vitamins A, E and C that are convenient with human body [17, 18]. Mucus is produced by the glands in the dorsal and lateral foot epithelium and shows an adhesive property whereas, slime known as ‘trail’ mucus, is the secretion that snails leave behind during their movement and produced by the glands located in the ventral region of the foot sole. The main difference between mucus and slime is that mucus has more specific protein content that leads to its adhesive property [18]. Although many studies have been conducted regarding the bioactive effects of snail

secretion, there are limited research about the use of snail extracts in tissue engineering applications. Angulo *et al* fabricated gelatin/CHI scaffolds using freeze-drying method and loaded different amounts of snail (*H. aspersa*) mucus and aloe vera extracts in polymer matrix. Results indicated that extract loaded scaffolds showed potential for *in vitro* tissue development [19]. In another study, CHI/snail mucus films were fabricated to investigate how snail mucus affects physicochemical properties of CHI-based films [20].

Especially, with its collagen, elastin and GAG composition, *H. aspersa* secretions (mucus-slime extract) can be used as a potential bioactive agent for hard tissue (bone-cartilage) regeneration to mimic the tissue in terms of physical and chemical structure. The aim of the present study was to fabricate mucus and slime extract loaded bioactive CHI based scaffolds to enhance the physical characteristics of CHI matrix as well as inducing its bioactivity with extensive biological composition of *H. aspersa* secretions for hard tissue regeneration. Thus, mucus and slime extracts of *H. aspersa* was used for two different tissue regeneration (bone-cartilage) with their distinct characteristics. Fabricated mucus and slime incorporated scaffolds showed significant effects on morphological, physical and antimicrobial properties of CHI matrix. Extract loading induced the *in vitro* bioactivity of Saos-2 and SW1353 cell lines on CHI scaffolds.

## 2. Material and methods

CHI with medium molecular weight powder was purchased from Sigma-Aldrich and used for preparation of scaffolds. *H. aspersa* mucus extract (Medical Grade) Xi’an SR Bio-Engineering Co., Ltd, *H. aspersa* slime extract (Pharmaceutical Grade), Xi’an Nate Biological Technology Co., Ltd were obtained from a commercial in China. WST-1 cell proliferation reagent (BioVision Inc.), Enzyline PAL Optimise (Biomerieux, France) kit, Human Osteocalcin (OC/BGP) ELISA Kit (Elabscience), Hydroxyproline assay kit (Elabscience), human cartilage oligomeric matrix protein (COMP) Sandwich ELISA Kit (Elabscience), Proteoglycan detection kit (Amsbio, AMS Biotechnology) were used for *in vitro* assays. 4',6-diamidino-2-phenylindole (DAPI) (Sigma Aldrich) and Alexa Fluor 488 (Thermo Fisher Scientific) were used for fluorescence staining. Materials were used for histological stainings were Hematoxylin&eosin (H&E) (Mayer's), Masson Trichrome (Bio optica, 04–010802), Alizarin Red (Abcam, a146374), Alcian Blue Kit (Sciencecell 8378), Type I collagen (bs-10423R, Bioss) and Type II collagen (bs-0709R, Bioss). Alizarin Red S and von Kossa were purchase from Sigma, Aldrich. Minimum Essential Media (MEM) Eagle's (Capricorn Scientific) and all supplements (Lonza) were used for cell culture study.

## 2.1. Fabrication of chitosan-slime (CHI-S) and chitosan-mucus (CHI-M) scaffolds

CHI solution was prepared by dissolving CHI (1% wt) in 100 ml acetic acid (1% v/v) overnight for CHI control group. For CHICHI-M and CHI-S composite solutions, 1% wt CHI was dissolved in 80 ml acetic acid solution and slime or mucus powder (0.5% wt, 1% wt, 3% wt) dispersed in 20 ml acetic acid solution separately. Then, CHI solution and slime dispersion were blended in magnetic stirred overnight. Then CHI solution was placed into 24 well plate and frozen  $-20\text{ }^{\circ}\text{C}$  for 24 h. Lyophilization process was carried out at  $-46\text{ }^{\circ}\text{C}$ , 0.018 mbar vacuum for 48 h to obtain porous structure.

## 2.2. Characterization of scaffolds

### 2.2.1. Scanning electron microscopy (SEM) analysis

Morphology of the scaffolds and the effect of slime and mucus extracts on the pore structure were observed by SEM. Scaffolds were coated with a thin gold layer under argon gas before analysis. SEM analysis was performed using Quanta FEG SEM. Average pore size of the scaffolds was determined with Image J Software. Pore size distribution of scaffolds was investigated with Minitab Software and depicted as histogram.

### 2.2.2. Open porosity measurement by liquid displacement method

Open porosity % of scaffolds ( $n = 3$ ) were determined by liquid displacement method. Scaffolds were placed in tubes containing ethanol ( $V_1$ ) and incubated in vacuum oven to remove air bubbles in the porous structure.  $V_2$  is indicated the total volume of scaffold with ethanol. Then the tubes were removed from the vacuum oven and the elevation levels of ethanol were determined. Finally, the scaffolds were taken from the tubes and the ethanol levels were measured ( $V_3$ ). Open porosity % of the scaffolds was calculated with equation is defined as:

$$\varepsilon = \frac{V_1 - V_3}{V_2 - V_3} \times 100. \quad (1)$$

### 2.2.3. Water absorption capacity

First, the dry weight ( $W_0$ ) of three scaffolds from each group ( $n = 3$ ) was measured before the swelling tests and the scaffolds were neutralized by incubating in 1 M NaOH solution for 30 min to inactivate the open bonds. After neutralization, the samples were washed twice with 1X phosphate-buffered saline (PBS) solution. Then the scaffolds placed in 1X PBS at  $37\text{ }^{\circ}\text{C}$  for 1 h, 24 and 48 h periods. Using filter paper the excess water on the scaffolds surface was removed and the scaffolds were weighed ( $W_1$ ). The swelling ratio was determined by time-dependent weight change before and after incubation in PBS solution. The equation that calculates the water absorption capacity % is defined as:

$$\text{Swelling \%} = \frac{W_1 - W_0}{W_0} \times 100. \quad (2)$$

### 2.2.4. Compression test

Mechanical properties of scaffolds were determined with compression test using TA-XT Plus Texture Analyzer. Compression test was carried out according to ASTM D 5024-95a standard. Five specimens were used for each group. Compression was performed with  $5\text{ mm min}^{-1}$  (for 0.5% and 1% scaffolds group) and  $50\text{ mm min}^{-1}$  (for 3% scaffolds group) cross head speed up 75% strain. Elastic modulus and maximum stress were calculated for each group.

### 2.2.5. Fourier transform infrared spectroscopy (FTIR)

The chemical structure, characteristic peaks of CHI and snail secretion extracts and the interaction of CHI with slime and mucus extracts were determined by FTIR (Perkin Elmer) at wavenumber range of  $650\text{--}4000\text{ cm}^{-1}$ .

### 2.2.6. Enzymatic degradation of scaffolds

Enzymatic degradation experiments were carried out at  $37\text{ }^{\circ}\text{C}$  with 1X phosphate buffer solution (PBS, pH 7.4) containing  $1.5\text{ }\mu\text{g ml}^{-1}$  lysozyme to mimic its concentration in human serum [21]. Sodium azide (0.01%) was added to enzymatic solution to inhibit microbial contamination. The enzymatic medium was changed three times a week prevent the loss of enzymatic activity. Weight loss % of samples ( $n = 3$ ) were measured for 7, 14, 21 and 28 d of incubation periods. The extent of enzymatic degradation was expressed as weight loss % of the dried scaffolds ( $w_0$ ) after lysozyme treatment ( $w_1$ ). Enzymatic biodegradation was indicated by weight loss % calculated using equation (3) as shown below;

$$\text{Weight loss \%} = \frac{W_0 - W_1}{W_0} \times 100. \quad (3)$$

### 2.2.7. Antimicrobial activity

Antimicrobial activity of snail secretions was determined with disc diffusion method on *Escherichia coli* (*E. coli*), *Staphylococcus aureus* (*S. aureus*), *Staphylococcus epidermidis* (*S. epidermidis*), *Streptococcus mutans* (*S. mutans*) and *Pseudomonas fluorescens* (*P. fluorescens*). Frozen microbial stocks were activated at  $37\text{ }^{\circ}\text{C}$  for overnight before disc diffusion tests. Cultured microorganisms were suspended in PBS solution and turbidity was adjusted to McFarland 0.5. Bacteria were inoculated on the Mueller-Hinton agar plates. The empty discs (14 mm diameter,  $n = 3$ ) were placed on the inoculated agar plates in sterile environment and.  $20\text{ }\mu\text{l}$  of mucus and slime extract solutions (0.5%, 1%, 3%) were dropped on empty discs (OxoidTM). Amoxicillin antimicrobial susceptibility discs ( $10\text{ }\mu\text{g m l}^{-1}$ , OxoidTM) were placed on agar plates as positive control groups. Petri dishes were incubated for 24 h at  $37\text{ }^{\circ}\text{C}$  (*P. fluorescens* inoculated

plates were incubated at 25 °C). At the end of incubation period, antimicrobial zones formed around the discs, and the diameters of the zones were measured in three replications, and the average zone diameters were calculated. After the determination of antimicrobial activity of secretions, scaffolds were incubated in 1X PBS solution overnight at 37 °C to mimic the human body. Then these solutions were investigated with disc diffusion method against *S. epidermidis* and *P. Fluorescens* to determine the effect of snail extracts released from scaffolds.

### 2.3. In vitro cytocompatibility studies

Saos-2 human osteosarcoma and SW1353 human chondrosarcoma cell lines were sub-cultivated with MEM Eagle's medium and used for *in vitro* studies.

#### 2.3.1. Cytotoxicity test

*In vitro* cytotoxicity of bioactive scaffolds was determined using indirect extraction method according to ISO-10993 standard. Scaffolds were extracted by incubating in cell culture media 24 h at 37 °C. Extraction media of each group was used as culture medium for cell viability. WST-1 colorimetric viability assay was used to measure the optical density at 440 nm and absorbance data was normalized to the cell viability. Cell viability was measured for 24, 48 and 72 h. The equation of the cell viability % is defined as:

$$\begin{aligned} \text{Cell viability \%} &= \frac{\text{Average absorbance value of treated samples}}{\text{Average absorbance value of control}} \\ &\times 100. \end{aligned} \quad (4)$$

#### 2.3.2. Cell proliferation of scaffolds

Cell proliferation on scaffolds ( $n = 3$ ) were incubated at 37 °C, 5% CO<sub>2</sub> for 28 d of incubation. Scaffolds were incubated in 70% (v/v) ethanol solution overnight for sterilization. Before cell seeding, scaffolds were washed thrice with 1X PBS solution to remove ethanol solution and conditioned with cell culture medium for 2 h. Then, Saos-2 and SW1353 cells were seeded on scaffolds at a density of  $2 \times 10^6$  cell ml<sup>-1</sup> and scaffolds were incubated 4 h at 37 °C for cell attachment. MEM and MEM Eagle's supplemented with 10% FBS, 1% L-glutamine and 1% penicillin-streptomycin were used for cultivation of Saos-2 and SW1353 cell lines. Cultivation medium was changed twice a week. The colorimetric WST-1 cell viability kit was used to detect cellular metabolic activity. The absorbance was measured by plate reader (Varioskan Flash, ThermoFisher Scientific) at 440 nm wavelengths.

#### 2.3.3. Cell attachment and spreading on scaffold

Saos-2 and SW1353 cells were seeded on scaffolds and incubated for 7 d to observe cell attachment and spreading. After incubation, cell fixation was carried

out with 3.7% paraformaldehyde (v/v) in PBS solution for 20 min at room temperature. DAPI and Alexa fluor 488 stains were used to detect nuclei and cytoskeleton. After fixation, samples were washed with 1X PBS solution and fixed cells were permeabilized with 0.1% Triton X-100 for 5 min. The stained cells were examined and visualized with fluorescent microscopy (ZEISS Observer Z1).

#### 2.3.4. Alkaline phosphatase (ALP) activity and osteocalcin (OC) secretion

The osteogenic culture medium of Saos-2 cells was prepared by adding 1% beta glycerophosphate and 0.1% ascorbic acid to MEM supplemented with 10% FBS, 1% L-glutamine, 1% penicillin-streptomycin, Saos-2 cells seeded on CHI, CHI-M and CHI-S scaffolds were cultured for 28 d with osteogenic medium. The ALP activity of scaffolds ( $n = 3$ ) was determined using the Enzyline PAL Optimise (Biomerieux, France) kit at 7, 14, 21 and 28 d. OC secretion ( $n = 3$ ) was evaluated using Sandwich-ELISA assay (Human OC/BGP (Osteocalcin) ELISA Kit, Elabscience) at 21 and 28 d.

#### 2.3.5. Alizarin red and von Kossa staining

Alizarin red staining is commonly used to detect and quantify calcium, while von Kossa staining is used to visualize phosphate, within the deposited mineral [22]. Firstly, cells cultivated on scaffolds were fixed with 3.7% paraformaldehyde for 20 min at room temperature. The scaffolds were then washed three times with distilled water and incubated for von Kossa staining. For von Kossa staining, 1% (w/v) silver nitrate solution (Sigma-Aldrich) was added on scaffolds and incubated under UV for 30 min. Then, washed three times with distilled water. After washing, scaffolds were kept in 5% sodium thiosulfate (Sigma-Aldrich) for 5 min to eliminate unreacted silver. Scaffolds were incubated with 2% alizarin red solution (pH 4.1) for 30 min at room temperature and in the dark for Alizarin Red staining. Afterwards, the stain residues were removed by washing several times with distilled water. Calcium and phosphate deposition on the scaffolds viewed by stereomicroscope (Olympus SOIF DA 0737). In addition, calcium deposition was determined with alizarin red extraction ( $n = 3$ ) by spectrophotometer analysis at 450 nm.

#### 2.3.6. Hydroxyproline (HP) assay

Total HP content of Saos-2 and SW1353 cells incubated on scaffolds ( $n = 3$ ) was determined with colorimetric HP assay kit (Elabscience) according to the manufacturer's protocol and measured spectrophotometrically at 550 nm. HP content was measured at 14, 21 and 28 d for SW 1353 cell line and 28 d for Saos-2 cell line.

### 2.3.7. Determination of cartilage oligomeric matrix protein (COMP)

COMP secretion of SW1353 cells in culture media ( $n = 3$ ) was measured at 3 and 7 d using Human COMP Sandwich ELISA assay (Elabscience) according to the manufacturer's protocol.

### 2.3.8. Glycosaminoglycan (GAG) assay

Total GAG content of SW1353 cells incubated on scaffolds ( $n = 3$ ) was determined with spectrophotometric proteoglycan detection kit (Amsbio, AMS Biotechnology) at 14, 21 and 28 d of incubation. Papain extraction method was used according to the manufacturer's protocol. Scaffolds were incubated with papain solution (papain, dithiothreitol (DTT), ethylenediamine tetraacetic acid) EDTA) for 6 h at 60 °C. After incubation step, dimethylmethylene blue DMMB solution was added and GAG content was measured spectrophotometrically at 530 nm.

## 3. Histological and immunohistochemical analyses

### 3.1. Histological analysis

The morphology, distribution, adhesion, and extracellular matrix ECM production of the scaffolds ( $n = 1$ ) were evaluated with histochemical and immunohistochemical staining at 7 and 28 d. The samples were fixed 3%, 7% formaldehyde solution and embedded paraffin blocks. 5  $\mu\text{m}$  sections were taken with a microtome. After the sections were deparaffinized, H&E, Safranin O/Fast Green, Alcian Blue, Alizarin Red S and Masson's trichrome staining were performed. H&E staining was performed to show the general morphology and Masson Trichrome (blue) was used to detect the presence of collagen. Alizarin Red S staining was performed to indicate calcium accumulation whereas, Alcian Blue (green/light blue) and Safranin O/Fast Green (red/purple) staining were used to indicate the presence of GAG in the extracellular matrix.

### 3.2. Immunohistochemical analysis

Immunohistochemical analyses were performed with Collagen Type I and II staining at 7 and 28 d of incubation. In immunohistochemical evaluation ( $n = 1$ ), 5  $\mu\text{m}$  sections were taken and treated with Type I collagen (bs-10423R, Bioss) and Type II collagen (bs-0709R, Bioss) after the dehydration stage. The samples incubated at +4 °C for one night and Diaminobenzidine kit was used to make the reaction visible. Then the samples examined with light microscopy at x100 magnification (Olympus BX51) after ground staining with Mayer's hematoxylin. Immunoreactivity intensity was performed by semi-quantitative scoring as no staining (0; -), low staining (1; +), moderate staining (2; ++) and severe staining (3; +++) [23, 24].

### 3.3. Statistical analysis

In this study, samples were analyzed in characterization tests with three replications. Five samples from each group were used for the mechanical experiment. The experimental data was given with the standard error of mean. Statistical analyses were carried out using One-way ANOVA and Two-way ANOVA with Tukey's multiple comparison test statistical methods ( $p < 0.05$ ).

## 4. Results and discussion

### 4.1. Characterization of scaffolds

#### 4.1.1. Morphology and structure of scaffolds

Pore size and pore structure of scaffolds are important factors for mechanical properties, cell adhesion, cell proliferation and tissue formation. Connection between pores facilitate the attachment of cells to the scaffold. In addition, porosity and average pore diameter play a critical role in the transfer of oxygen and nutrients supplied by the bloodstream, providing the appropriate environment for vascularization. The optimum pore size should be 200–350  $\mu\text{m}$  for osteoinduction, and 150–200  $\mu\text{m}$  for chondrocyte cells to attach and grow on the scaffold [25–30]. In this study, morphology and porosity of CHI, CHI-M and CHI-S scaffolds were determined by SEM. SEM images show that pore distribution of the scaffolds was homogenous and transitions between the pores were distinct (figures 1 and 2). Average pore diameters of scaffolds were measured using Image J software (figures 1 and 2). The pore diameters of the scaffolds were found to be suitable for the cartilage and bone cells to attach and proliferate. Compared with CHI matrix, composite scaffolds prepared by using snail secretions have reduced pore diameters but increased wall thickness. Thus, increased surface area provided a more favorable environment for cell adhesion and proliferation.

Highly porous scaffolds are required to allow for cells to infiltrate and attach to the scaffold, to provide a high surface area-to-volume ratio for polymer-cell interactions, and to obtain minimal diffusion constraints during cell culture. Past research has stated that a scaffold porosity of greater than 90% is important for tissue engineering applications. However, researchers have used scaffolds with porosities ranging from 55% to 74% for bone growth due to increased mechanical properties at lower porosities [31]. Porosity should be lower (71%) to better mimic the natural cartilage structure [32]. Porosity can also indirectly affect cell response by altering the fluid shear forces on the cell. While it is difficult to recapitulate the *in vivo* environment exactly in cell culture, studies have shown that cells are indeed influenced by mechanical forces resulting from fluid flow, and that these flows are altered based on scaffold porosity. Additional studies have shown the importance of

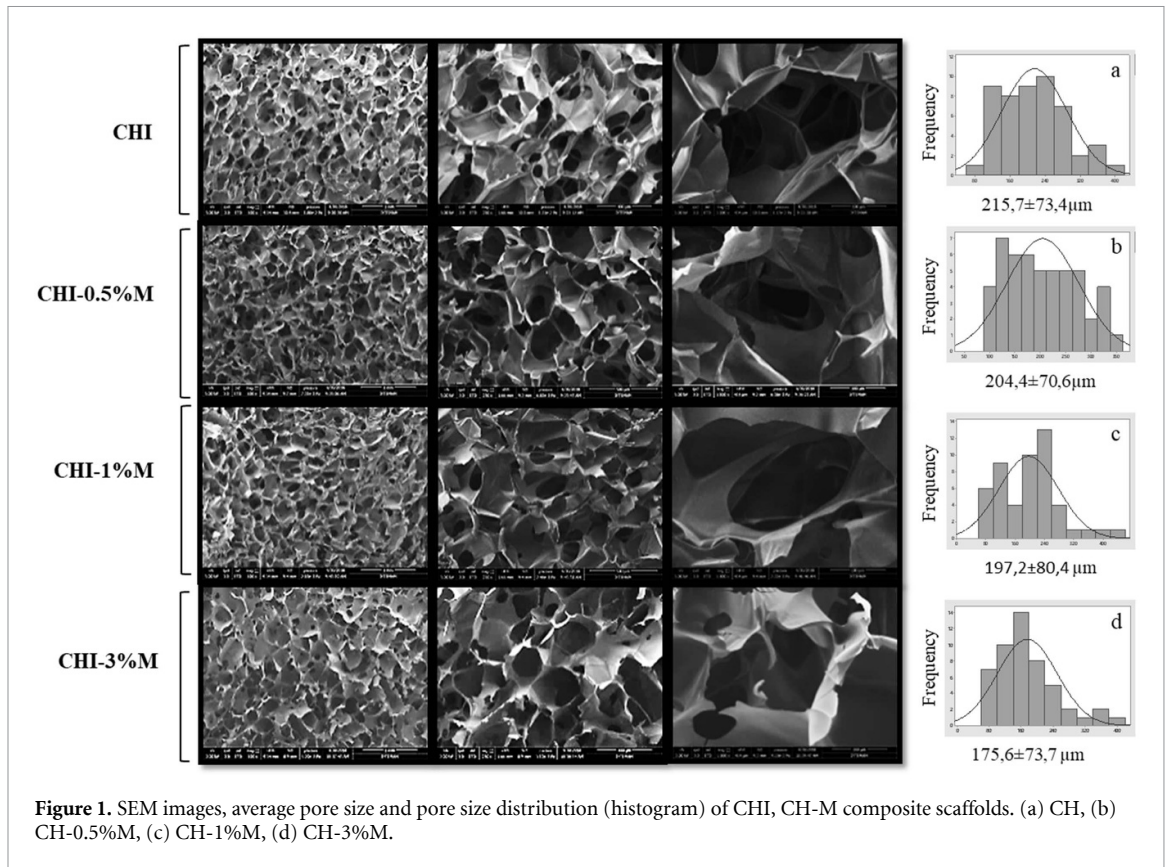


Figure 1. SEM images, average pore size and pore size distribution (histogram) of CHI, CH-M composite scaffolds. (a) CH, (b) CH-0.5M, (c) CH-1M, (d) CH-3M.

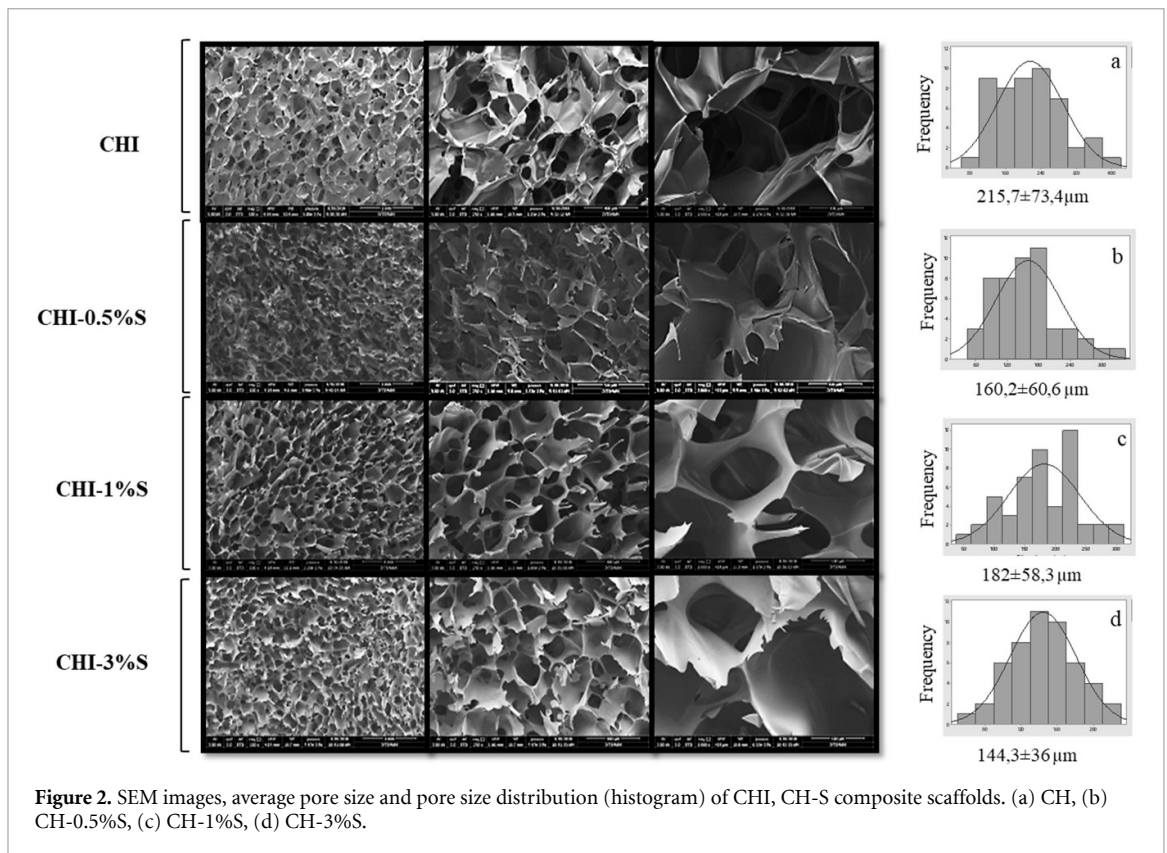


Figure 2. SEM images, average pore size and pore size distribution (histogram) of CHI, CH-S composite scaffolds. (a) CH, (b) CH-0.5S, (c) CH-1S, (d) CH-3S.

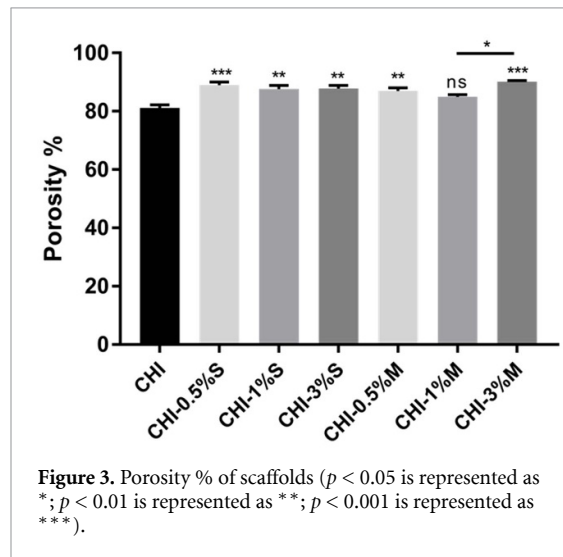
smaller micropores and the role of morphology in facilitating protein adsorption [33].

Open porosity % of scaffolds were determined with liquid displacement method and data was given

in table 1. In this study, over 80% high porosity was obtained in all groups of scaffolds with mucus and slime loaded. Open porosity % data of scaffold groups were found statistically significant except CHI-1%M

**Table 1.** Porosity % of scaffolds determined by liquid displacement method.

Scaffold groups	Porosity %
CHI	81 ± 0.9
CHI-0.5%S	89 ± 0.9
CHI-1%S	88 ± 1
CHI-3%S	88 ± 0.8
CHI-0.5%M	87 ± 0.8
CHI-1%M	85 ± 0.6
CHI-3%M	90 ± 0.3

**Figure 3.** Porosity % of scaffolds ( $p < 0.05$  is represented as \*;  $p < 0.01$  is represented as \*\*;  $p < 0.001$  is represented as \*\*\*).

when compared with CHI (figure 3). Mucus and slime secretions added to the scaffolds increased the porosity rate. In addition, CHI scaffolds loaded with mucus and slime extract were observed to have a homogeneous microstructure. The homogeneity in morphology also positively affected the mechanical strength of the scaffolds.

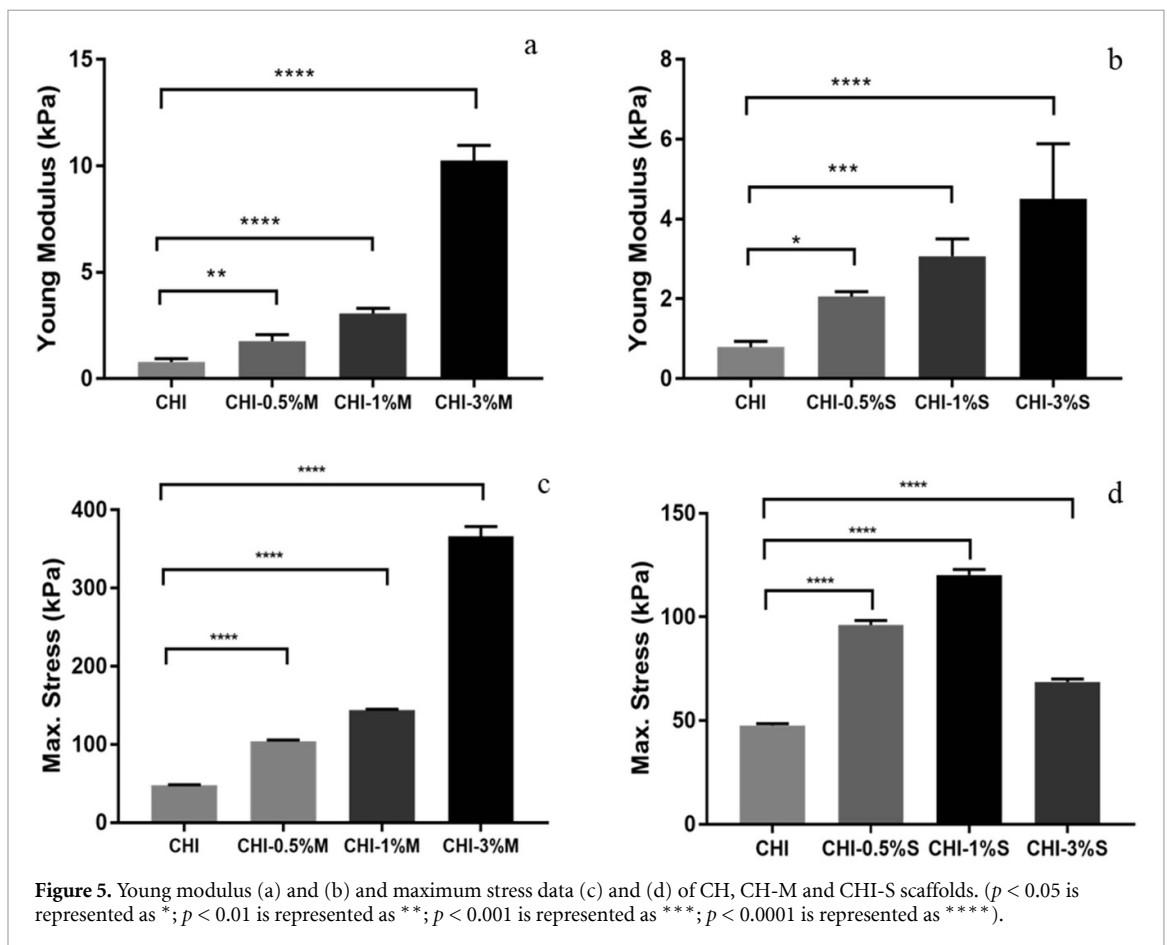
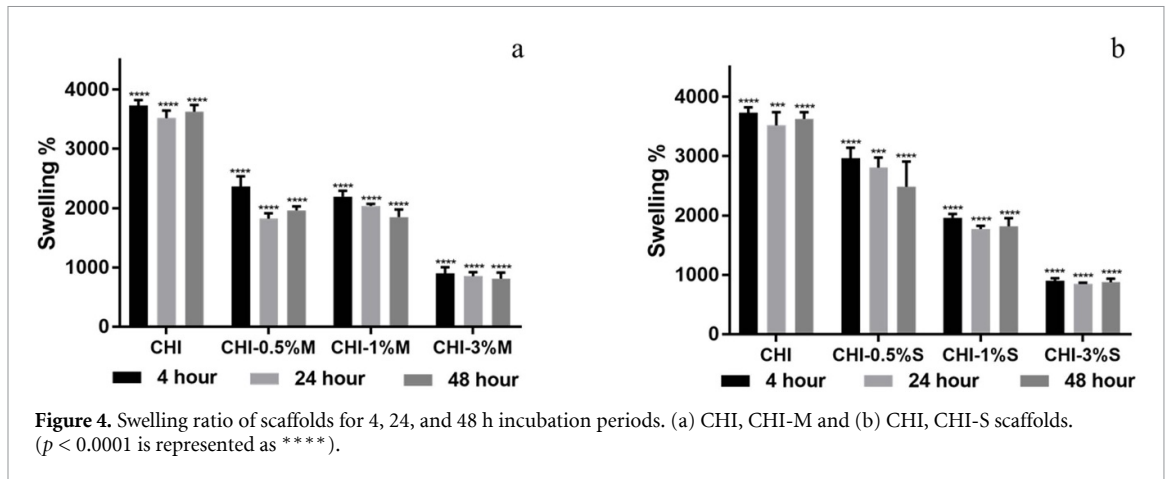
#### 4.1.2. Water absorption capacity of scaffolds

The water absorption property of the raw materials influences not only the maintenance of scaffolds shape but also affects the cell growth. Swelling behavior and structural stability of scaffolds are critical to their practical use in tissue engineering [34]. In addition, the swelling behavior of scaffolds plays an important role in keeping water, adsorbing body fluids and transferring nutrients and metabolites into cells. Swelling behavior of a scaffold depends strongly on the pH value of the implantation site. When the scaffold is placed on the defect site in the body, it first contacts with body fluid and triggers protein adsorption, then cell adhesion occurs on the material surface. Most natural polymers, including CHI, swell readily in biological fluids. Swelling ratios of scaffolds were calculated using equation (2) and results shown in figure 4. As an increase in the extract loading, the swelling ratio decreased due to the decrease in pore size of the scaffolds. With the smallest pores of 3% slime and mucus loaded CHI composites, (CHI-3%S and CHI-3%M), the lowest swelling ratio was

observed as the water uptake was only influenced by pore size. Although snail secretion incorporation decreased water absorption capacity and swelling ratio of CHI-M and CHI-S, the composites still have a high % swelling ratio of 1000–3000. In the study of Angulo *et al*, the water absorption capacity of snail mucus loaded CHI/gelatin scaffolds was investigated and it was found that the water absorption capacity of 0.07% snail mucus loaded scaffolds showed higher swelling ratio results (600%–1000%) than 0.15% snail mucus loaded scaffolds (600%–800%) during incubation time [19]. This indicated that increasing mucus extract concentration decreased the water absorption capacity.

#### 4.1.3. Mechanical properties of scaffolds

Mechanical strength is another feature that should be taken into consideration in the design of the scaffold. The scaffolds must be durable enough to supply the stress given by natural tissue. Also, the pore size, pore distribution and microstructure homogeneity of the scaffolds are highly effective on the mechanical properties. Mechanical properties of scaffolds were determined with compression tests (TA-XT Plus Texture Analyzer) according to ASTM D 5024-95a standard and results were indicated in figure 5. Mucus and slime extracts had a positive effect on Young's modulus. Results showed that increasing mucus and slime concentration from 0.5% up to 3% enhanced the modulus of CHI scaffold. The scaffold groups with the highest wall thickness showed the highest mechanical strength. However, 3% slime incorporated CHI scaffold showed fractures during compression test due to the separation of extract from the polymer matrix. Thus, CHI-3% slime scaffold exhibited a brittle behavior in compression test. Compression moduli differences between groups were found statistically significant. The mucoadhesive characteristics of *H. aspersa* snail mucus extract arises from its glue protein content which causes gel formation with the polymer content in its structure and effect gel mechanics [35]. Thus, increasing mucus concentration enhanced the mechanical properties as Young's modulus and maximum stress of CHI matrix. Mucus and slime incorporated scaffolds increased the maximum stress from 45.12 to 129.21 kPa (CHI-1%M) and 403.94 kPa (CHI-3%S). Young Modulus of CHI scaffold increased from 0.66 to 6.40 kPa (CHI-3%S) and 11.31 kPa (CHI-3%M). Angulo *et al* fabricated the snail mucus loaded CHI/gelatin scaffolds with different ratio (0.07% and 0.15%) and investigated the mechanical properties of composite scaffolds. They found the highest elastic modulus value for control group CHI/gelatin scaffolds as 0.04 MPa whereas, among the composite groups, 0.15% snail mucus and aloe vera extract loaded scaffolds showed the higher elastic modulus as 0.1 MPa compared to 0.07% extract loaded group (0.03 MPa) [19].



#### 4.1.4. FTIR analysis

FTIR analysis was performed for the chemical characterization of the scaffolds and snail secretion extracts (figure 6). In this research, characteristic bands of CHI were observed in the spectra of CHI-M and CHI-S blend. The main bands appearing in the spectrum of CHI is due to N–H bending in amine groups at  $1544\text{ cm}^{-1}$ , C–O stretch of acetyl group in amide II bonds at  $1640\text{ cm}^{-1}$ , amide III bonds at  $1377\text{ cm}^{-1}$  respectively [7, 36]. The region from  $1151$  to  $1024\text{ cm}^{-1}$  is characteristic band of C–O–C linkage [7]. Peaks at  $2867$  and  $2924\text{ cm}^{-1}$  are

the typical C–H stretch vibrations (indicated with black arrow). Finally, the C–N print band appears  $896\text{ cm}^{-1}$  [37, 38].  $1640$  and  $1540\text{ cm}^{-1}$  band regions are represented Amide bands in *H. aspersa* mucus (indicated with black arrow). This band region is also associated with proteinaceous core of GAGs and proteoglycan molecules [39]. Amide band of mucus extract showed at  $1641\text{ cm}^{-1}$ . Band region at  $1236$  and  $1000\text{ cm}^{-1}$  showed the sulfate groups and this may confirm to sulfated GAG content in mucus extract (indicated with red arrow) [12, 40]. Also,  $704$  and  $1075\text{ cm}^{-1}$  showed characteristic C=O



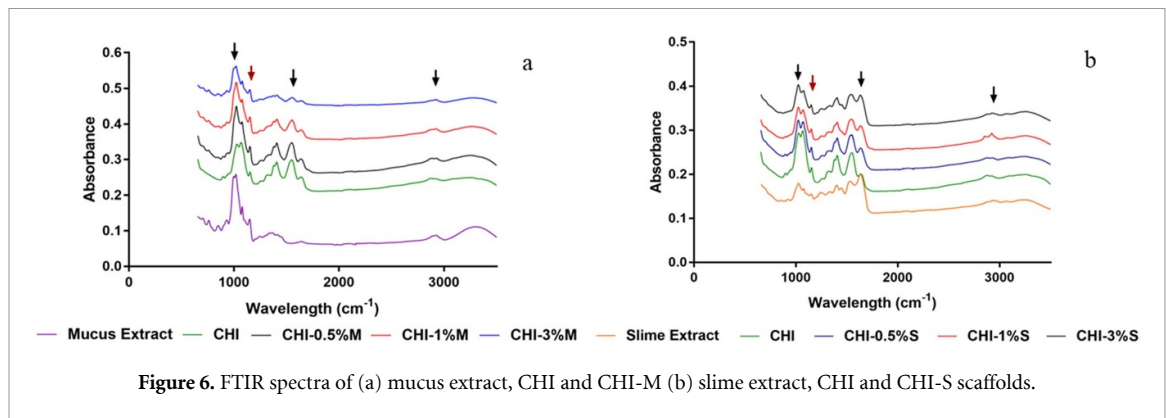


Figure 6. FTIR spectra of (a) mucus extract, CHI and CHI-M (b) slime extract, CHI and CHI-S scaffolds.

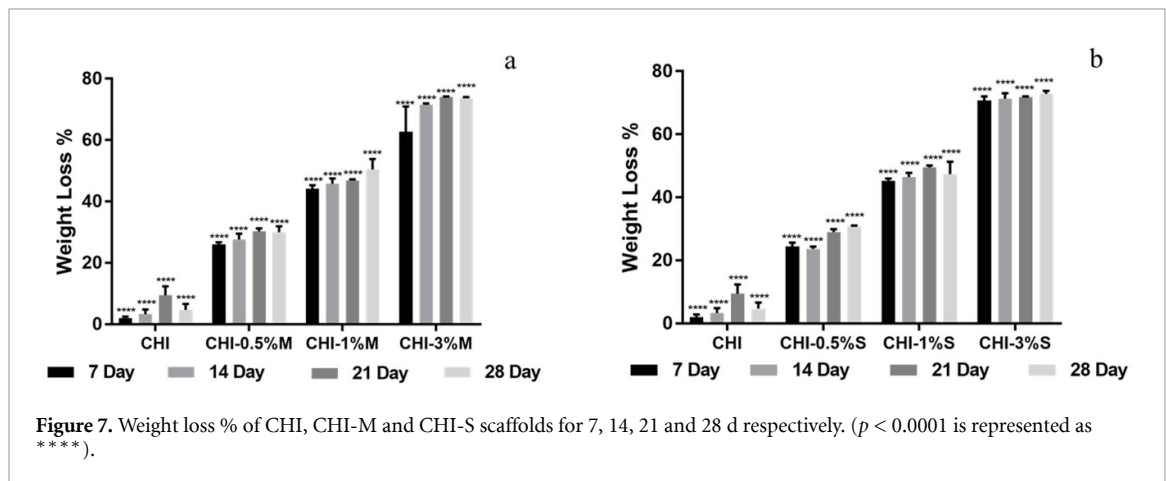


Figure 7. Weight loss % of CHI, CHI-M and CHI-S scaffolds for 7, 14, 21 and 28 d respectively. ( $p < 0.0001$  is represented as \*\*\*\*).

stretching vibration (indicated with black arrow), C–O formation at  $1202\text{ cm}^{-1}$ , and C–H alkanes group at  $2924\text{ cm}^{-1}$  of Vitamin E content in mucus extract [41]. There is limited literature study concerning to investigation of *H. aspersa* snail extract and *H. aspersa* extract is generally considered as mucus secretions. Thus, chemical and physical characterizations are determined for mucus secretion due to the chemical similarity of mucus and slime contents. Amide band of slime extract showed at  $1629\text{ cm}^{-1}$  (indicated with black arrow).  $920$  and  $1076\text{ cm}^{-1}$  showed characteristic C=O stretching vibration (indicated with black arrow), C–O formation at  $1202\text{ cm}^{-1}$ , and C–H alkanes group at  $2928\text{ cm}^{-1}$  of Vitamin E content in slime extract (indicated with black arrow). Sulfate groups in slime extract appearing at  $1238$  and  $1020\text{ cm}^{-1}$ . According to IR Table  $1327\text{ cm}^{-1}$  peak showed strong C–N stretching and peaks at  $1401$  and  $1444\text{ cm}^{-1}$  are determined as C–H bending (indicated with red arrow).

Addition of M and S extracts provokes a general broadening of the spectra, which assume characteristic features of the spectrum of M and S powder. The band at  $1015$  and  $1075\text{ cm}^{-1}$  at the spectra of CHI-M scaffolds occurred interaction of CHI and mucus extract. Bands observed at  $1020$  and  $1076\text{ cm}^{-1}$  may occur due to the possible interaction of CHI and slime extract.

#### 4.1.5. Enzymatic degradation of scaffolds

Biodegradability is an important criterion to be considered in the design of any scaffold for long-term success. Biodegradation refers to the chemical process in which biomaterials implanted in a biological system gradually decay. This is accomplished by exposing the scaffolds to tissue fluids containing various enzymes and other active ingredients. Implanted graft materials degrade over time and initiate tissue formation. However, an optimum degradation rate is essential which must supply the growth rate in the implant area and sustainability of the new tissue. Lysozyme is the main enzyme in wound exudation fluid that could hydrolyze the  $\beta(1-4)$  glycosidic linkage in CHI [42]. CHI oligosaccharides are degradation product which has variable length. The degradation kinetics is inversely correlated to degree of deacetylation and highly deacetylated forms (e.g.  $>85\%$ ) exhibit the lowest degradation rates [43]. Degradation study was performed to observe the weight loss of the scaffolds which were incubated in enzymatic medium and depicted in figure 7. The enzymatic degradation first starts from the surface of the polymer. Then, degradation process of polymer matrix continues with hydrolytic and enzymatic degradation [44]. Thus, surface structure and morphology of the scaffolds are main factors to initiate the degradation process. The degradation rate of mucus and

**Table 2.** Zone diameters of snail secretions for *S. epidermidis*, *P. fluorescens*, *S. aureus*, *E. coli*, *S. mutans* bacteria.

Bacteria species	Snail secretions and concentration (w/v)	Zone diameter (mm)
<i>S. epidermidis</i>	Amoxicillin (control)	11 ± 0
<i>S. epidermidis</i>	Slime	0.5% —
		1% —
		3% 1 ± 0
<i>S. epidermidis</i>	Mucus	0.5% —
		1% —
		3% 1 ± 0
<i>P. fluorescens</i>	Amoxicillin (control)	15 ± 0
<i>P. fluorescens</i>	Slime	0.5% 1 ± 0
		1% 1 ± 0
		3% 1.35 ± 0.14
<i>P. fluorescens</i>	Mucus	0.5% 1 ± 0
		1% 1.5 ± 0
		3% 1.85 ± 0.27
<i>S. aureus</i>	Amoxicillin (control)	+
<i>S. aureus</i>	Slime	0.5% —
		1% —
		3% —
<i>S. aureus</i>	Mucus	0.5% —
		1% —
		3% —
<i>E. coli</i>	Amoxicillin (control)	+
<i>E. coli</i>	Slime	0.5% —
		1% —
		3% —
<i>E. coli</i>	Mucus	0.5% —
		1% —
		3% —
<i>S. mutans</i>	Amoxicillin (control)	+
<i>S. mutans</i>	Slime	0.5% —
		1% —
		3% —
<i>S. mutans</i>	Mucus	0.5% —
		1% —
		3% —

slime loaded scaffolds increased due to the morphological changes such as open porosity. The increase in mucus and slime concentration in polymer matrix accelerated the degradation rate due to the hydrophilic nature of extracts that induced the hydrolytic degradation (mucus increase the degradation rate from 4.7% to 73.6%, slime increase the degradation rate from 4.7% to 72.8%). In addition, open porosity of scaffolds increased with increasing extract concentration as indicated in table 1. For cartilage tissue, the biodegradation rate should be less. For this reason, it is thought that the biodegradation rate of the scaffolds can be reduced by using crosslinkers in the following research. Considering the degradation

rates, the suitability of tissue scaffolds for bone tissue regeneration can be investigated.

#### 4.1.6. Antimicrobial activity of mucus and slime

Garden snails *H. aspersa* from the family *Helicidae* are very well-known species of gastropod mollusk. The hemolymph from snails contains bioactive compounds as glycans, peptides, glycopeptides, proteins and it has been discovered in recent years. Among other species, *H. aspersa* was identified with having three subunits for hemocyanins. Dolashka *et al* investigated the antimicrobial activity of fractions isolated from the mucus of garden snail *H. aspersa* against different species of Gram (+) (*Propionibacterium acnes* strain 266 (IA) and *P. acnes* KPA171202) and two Gram (−) bacterium (*E. coli* NBIMCC and *Helicobacter pylori*) [45]. In addition, Pitt *et al* investigated the antimicrobial properties of *H. aspersa* mucus in their study. In studies conducted with many bacterial species, *H. aspersa* mucus has been shown to be effective against *Pseudomonas aeruginosa* bacterial strain. The study indicated that *H. aspersa* mucus was composed of proteins with molecular weights of 30 and 100 kDa and showed antimicrobial properties [16]. In this study, five different bacteria, *S. epidermidis*, *E. coli*, *S. aureus*, *S. mutans* and *P. fluorescens*, were used to investigate the antimicrobial properties of snail secretions. Zone diameters measured from disc diffusion tests were given in table 2. Snail secretion solutions prepared at the concentration of 0.5%, 1%, 3% were found to be effective against *P. fluorescens* and *S. epidermidis* bacteria (figure 8). *S. epidermidis* is a gram-positive bacterium and it cause infection on the surface of medical prostheses [46]. *P. fluorescens* is a gram-negative bacterium and non-pathogenic type of *P. aeruginosa* known as hospital germ [47]. For *P. fluorescens*, zones were formed at each ratio around the discs and zone diameter differences were found statistically significant (figures 10 (a) and (b)). Zone form only has been acquired of 3% snail secretion solution at *S. epidermidis* bacterium. However, zone diameter differences were not found statistically significant. If the experiments are repeated by increasing ratio, it might be that the effect of snail secretions on *S. epidermidis* bacteria species will increase. The diameters of the control discs were not measured in non-zone species. In addition to the snail extracts, scaffold release solutions were used to investigate the antimicrobial activity of CHI/mucus and CHI/slimes scaffolds with different extract concentrations. Scaffolds were incubated in 1X PBS solution overnight and these solutions were used with disc diffusion test. Results indicated that scaffolds released snail extracts effectively and showed antimicrobial activity. Release media showed bacteriostatic effect on *S. epidermidis* whereas, antimicrobial activity was observed against *P. fluorescens* (figure 9). Zone diameters were given in table 3 and

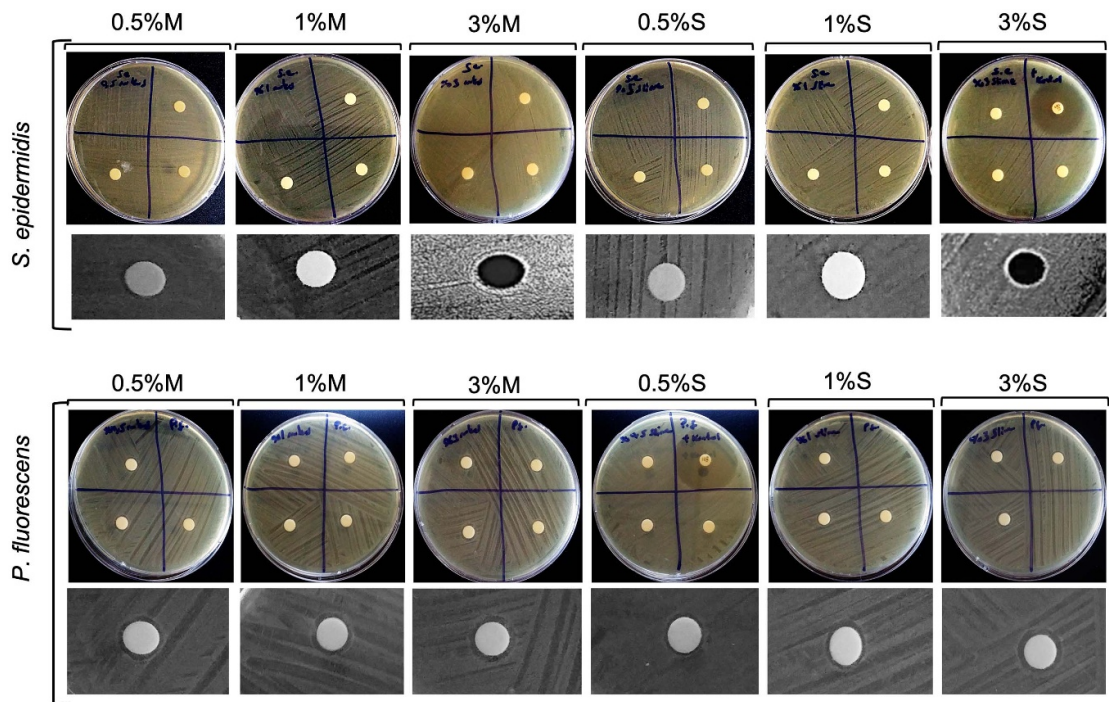


Figure 8. Disc diffusion zones of mucus and slime extract solutions on *S. epidermidis* and *P. fluorescens*.

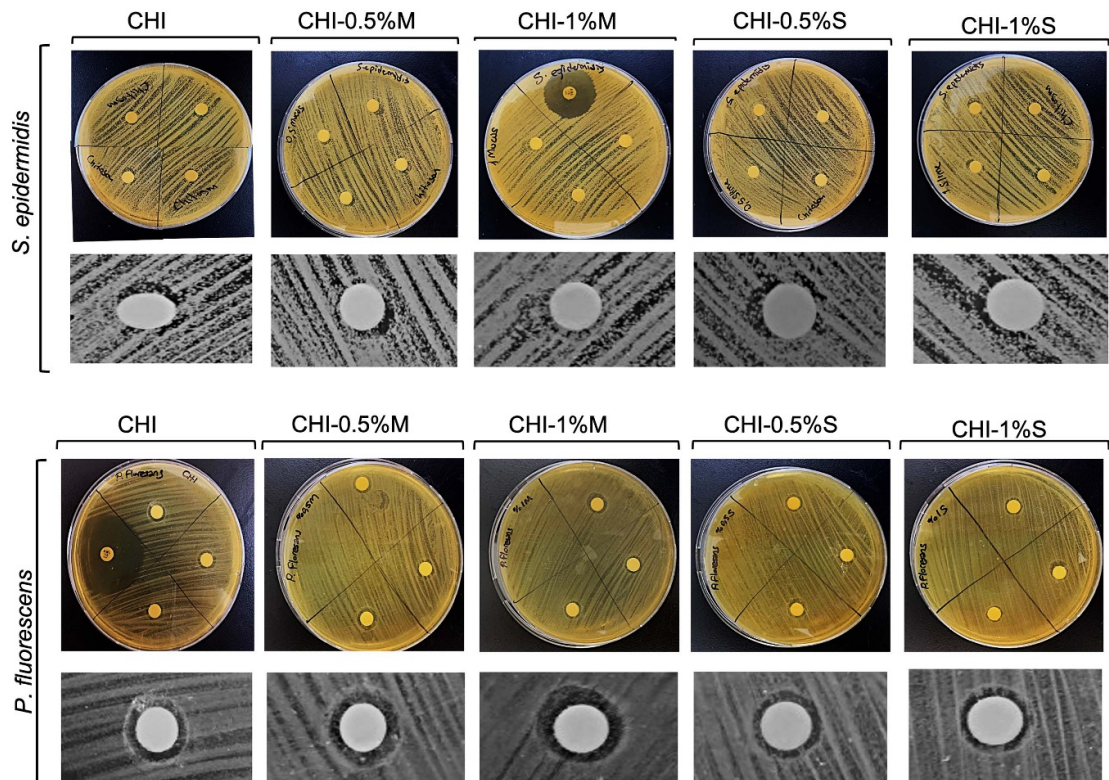


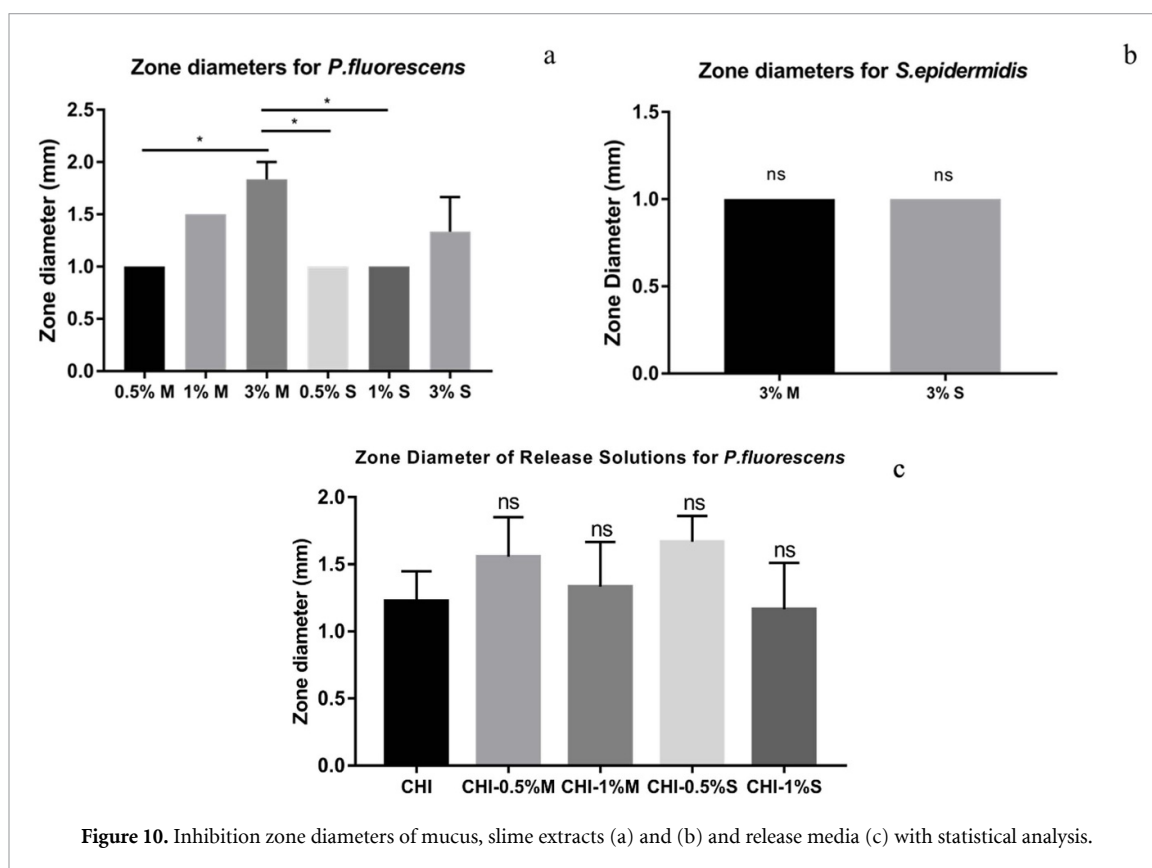
Figure 9. Disc diffusion zones of release solutions on *S. epidermidis* and *P. fluorescens*.

zone differences were depicted in figure 10(c). Maximum zone diameters were observed in CHI-0.5%S and CHI-0.5%M release media as 1.67 and 1.56 mm respectively. Increasing extract concentrations did

not positively affect the antimicrobial activity of scaffolds. This may arise from the structural changes of scaffolds with addition of snail extracts at higher concentrations. These alterations affect

**Table 3.** Zone diameters of release media of scaffolds for *S. epidermidis* and *P. Fluorescens*.

Bacteria species	Release solutions of scaffolds		Zone diameter (mm)
<i>S. epidermidis</i>	Amoxicillin (control)		15 ± 0
<i>S. epidermidis</i>	CHI		- (Bacteriostatic)
<i>S. epidermidis</i>	Slime	0.5%	- (Bacteriostatic)
		1%	- (Bacteriostatic)
			- (Bacteriostatic)
<i>S. epidermidis</i>	Mucus	0.5%	- (Bacteriostatic)
		1%	- (Bacteriostatic)
			- (Bacteriostatic)
<i>P. fluorescens</i>	Amoxicillin (control)		15 ± 0
<i>P. fluorescens</i>	CHI		1.23 ± 0.31
<i>P. fluorescens</i>	Slime	0.5%	1.67 ± 0.27
		1%	1.16 ± 0.49
			1.56 ± 0.41
<i>P. fluorescens</i>	Mucus	0.5%	1.56 ± 0.41
		1%	1.34 ± 0.47



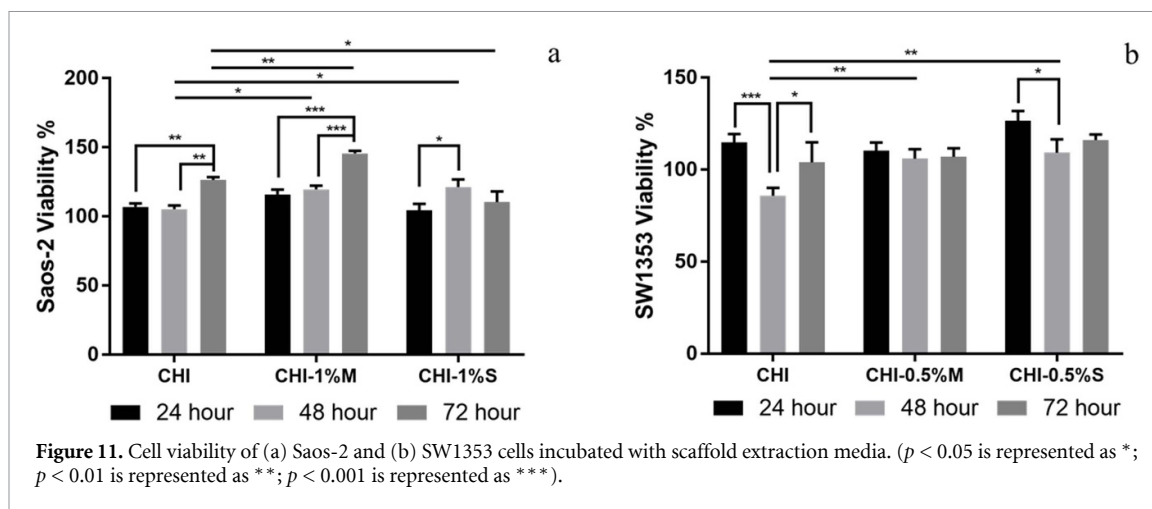
the release of bioactive extracts from the polymer matrix.

## 4.2. In vitro studies

### 4.2.1. Cytotoxicity

*In vitro* cytotoxicity of mucus and snail extract loaded scaffolds were investigated on Saos-2 and SW1353 model cell lines to mimic the bone and cartilage tissue response (Figure 11). High cell viability results were obtained after 72 h of incubation with extraction media. Mucus and slime extract incorporation did not show any toxic effect on Saos-2 and SW1353 cell lines. 1% mucus extract induced the Saos-2 cell viability at 72 h whereas, 1% slime extract incorporation showed different trend. Saos-2 cell viability increased up to 48 h but slightly decreased at 72 h. Cell viability of mucus and slime incorporated

groups showed significant difference with control group at 48 and 72 h of incubation. SW1353 cells were incubated with CHI-M and CHI-S scaffold extraction media with lower concentrations as 0.5%. High cell viability was obtained with extraction media at 72 h. SW1353 viability was found significantly higher at 48 h when compared to control group. Viability of slime incorporated group increased at 24 h and slightly decreased up to 72 h. This may arise from the mucoadhesive properties of slime extract on cell monolayer. Similarly, Kantawong *et al* investigated the cytotoxic effect of different *Achanica fulica* snail extract concentrations on dental pulp cells with 3-[4,5-dimethylthiazol-2-yl]-2,5 diphenyl tetrazolium bromide MTT assay and indicated that snail extract showed no toxic effect at 48 h of incubation [48]. In another study, snail mucus was incorporated



in CHI films and the effect of films on nonmalignant epithelial cells was assessed with *in vitro* cell viability assay. Results indicated that snail mucus had positive effect and induced the cell viability at 72 h of incubation [20].

#### 4.2.2. Cell proliferation of scaffolds

Saos-2 and SW1353 cell lines were used to study cell proliferation on extract loaded scaffold up to 28 d. Saos-2 cells proliferated on all scaffold groups with similar trend. The decrease in proliferation rate after 14 d of incubation result from the osteoblastic differentiation and biomineralization of cells on material surface (figure 14(a)). WST-1 results indicated that proliferation rate of SW1353 cells significantly increased on each group with incubation time whereas, SW1353 cells significantly proliferated on mucus and slime extract loaded scaffolds at 14 and 21 d of incubation compared to CHI control group (figure 16(a)). In literature, Angulo *et al* fabricated aloe vera and snail mucus loaded CHI/gelatin scaffolds for soft tissue regeneration. Results showed that aloe vera and mucus incorporation induced fibroblast growth and proliferation on CHI/gelatin scaffolds [49].

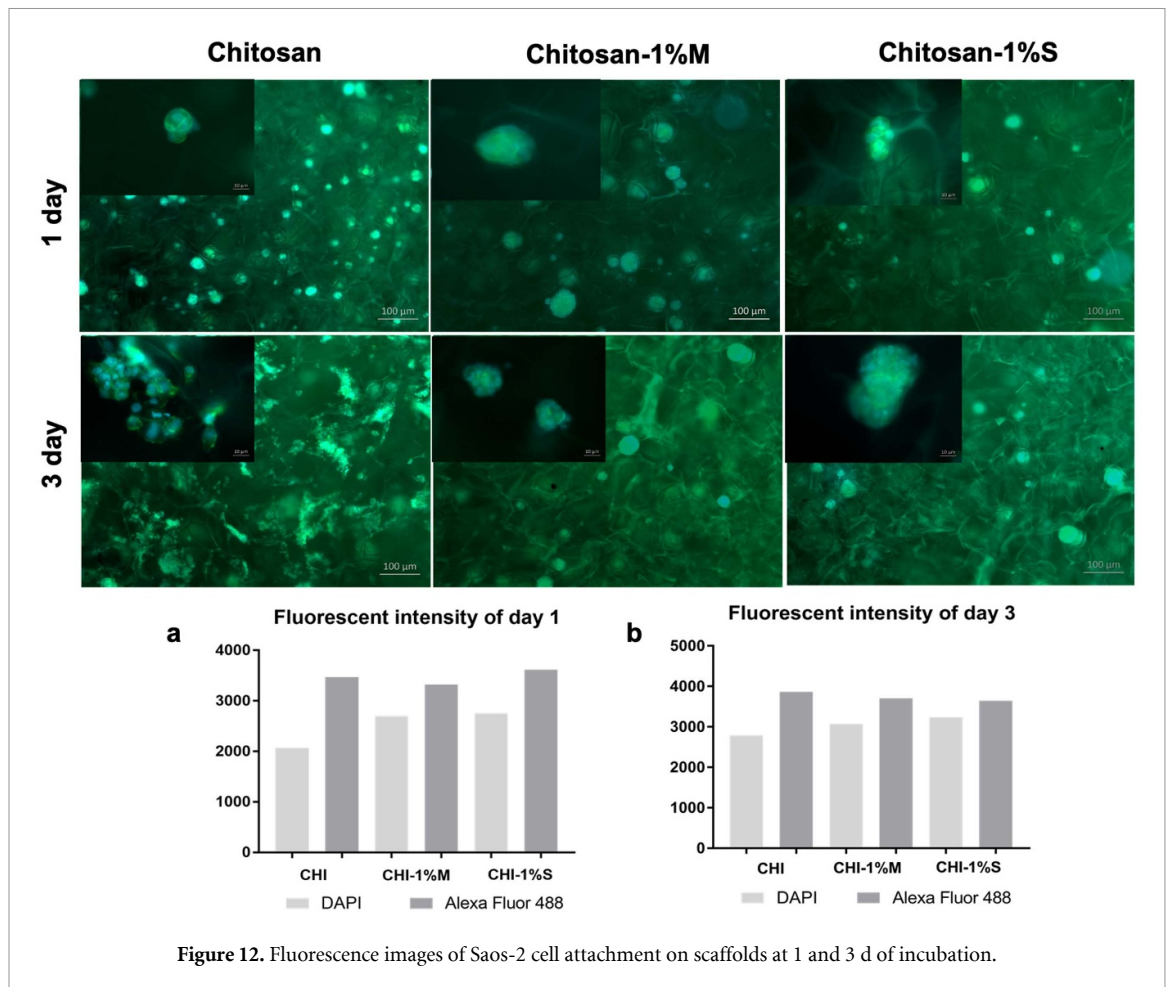
#### 4.2.3. Cell attachment and spreading on scaffolds

Cell-material interaction is the major step for cell bioactivity which depends on the surface characteristics of material that can be defined as topography, chemistry or surface energy. These surface characteristics effect the adsorption of biological molecules to the material surface to initiate cell attachment. Thus, inducing cell attachment and spreading on material surface can conduce to alter intracellular as well as osteogenic and chondrogenic activities [50]. Fluorescence images indicated that both Saos-2 and SW1353 cells attached on pore wall surfaces by forming clusters due to the effective cell to cell interaction (figures 12 and 13). In addition, mucoadhesive characteristics of mucus extract may affect

the cell attachment on material surface positively. Intensity data of fluorescence images (DAPI, Alexa Flour 488) indicated that mucus and slime extract loading enhanced the cell attachment. Similarly, Trapella *et al*, investigated the effect of Helix complex snail mucus extract on fibroblast attachment and proliferation. Extract treated fibroblasts exhibited morphological changes concerning the cytoskeleton organization [12].

#### 4.2.4. Alkaline phosphatase (ALP) activity, osteocalcin (OC) secretion and hydroxyproline content (HP)

ALP is a metalloenzyme that is expressed in several tissues. ALP activity is a key biomarker of early osteoblastic differentiation. ALP functions as an ectoenzyme bound to the plasma membrane through a phosphatidyl inositol-glycophospholipid linkage [51]. In this study, Saos-2 cell line was used to detect the effect of snail slime and mucus extract on ALP activity. Results revealed that both mucus and slime extracts induced extracellular ALP activity at the end of 28 d of incubation. The increase in ALP activity for all groups during incubation period was found statistically significant. In addition, 1% mucus incorporated group enhanced the ALP activity at 7th day compared to control CHI group (figure 14(b)). OC is known as an important late term biomarker as bone gla-protein due to the presence of three gamma-carboxyglutamic acid residues in its amino acid structure, and it is considered as the most abundant non-collagenous protein in bone tissue [52]. OC is generally preferred as biomarker for bone tissue formation. Because it is produced by osteoblasts at the beginning of biomineralization process. In this study, OC secretion of Saos-2 cells on scaffolds was determined with sandwich ELISA at 21 and 28 d of incubation. Results indicated that slime and mucus extract incorporation to CHI matrix induced the OC secretion significantly at 21st day when compared with control group CHI (figure 14(c)). HP, as a major amino acid in collagen is a unique marker because it occurs in



only collagen (13%) and elastin (about 1%). Therefore, it has been generally used for determining collagen amount present in a tissue. HP is formed through the co-translational hydroxylation of proline by the enzyme proline hydroxylase [53, 54]. For Saos-2 cells, HP content was measured at the end of the incubation (28 d) to determine the type 1 collagen content in culture (figure 14(d)). Absorbance results indicated that, HP content in slime loaded scaffolds enhanced collagen production, whereas CHI-M scaffolds did not significantly induced HP content. Statistical analyses showed that HP content of CHI-S scaffolds was found highest and significantly differed from CHI control group and CHI-M group.

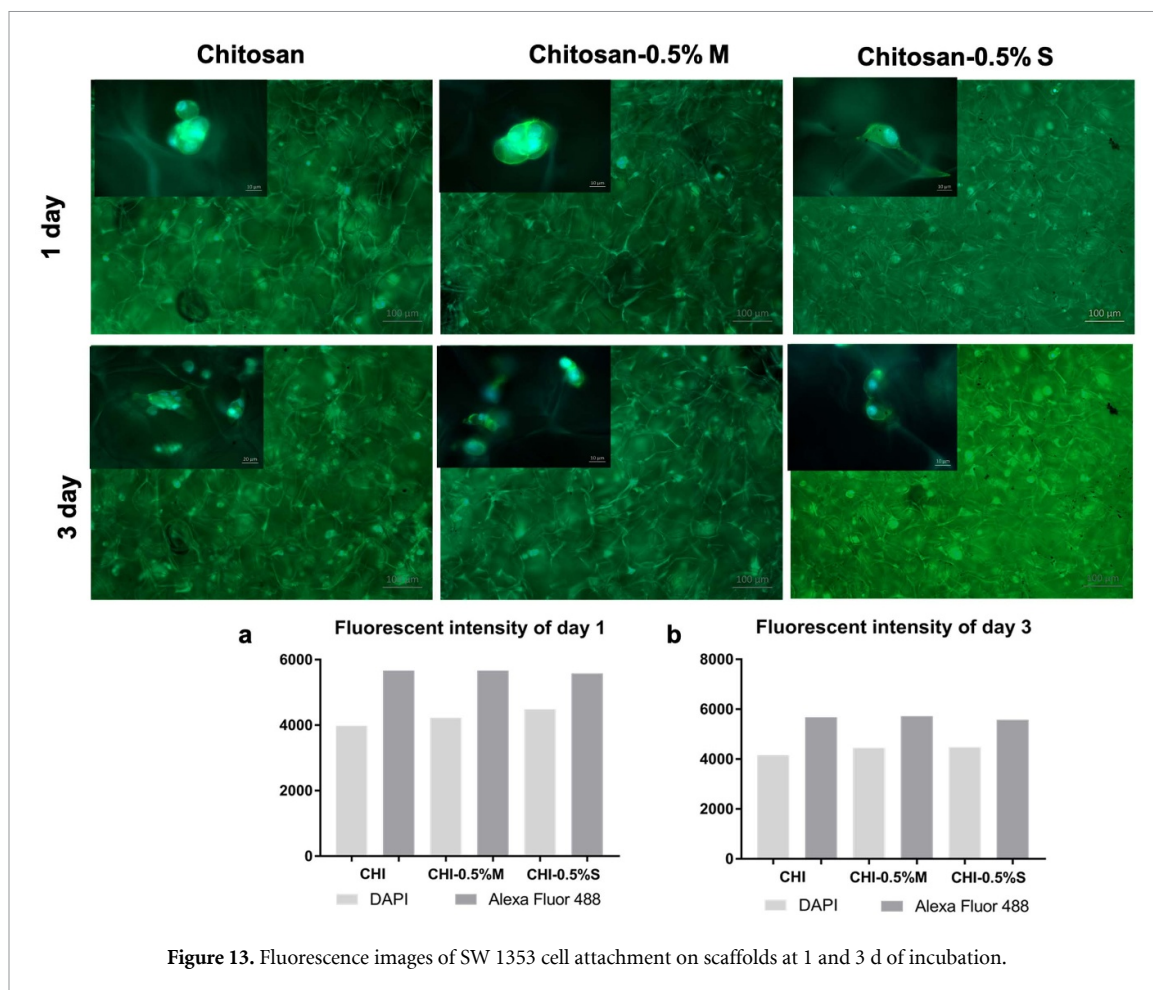
#### 4.2.5. Alizarin red and von Kossa staining

Alizarin Red and von Kossa staining protocols were performed to detect the calcium and phosphate deposition on scaffolds respectively. The scaffolds were observed under stereomicroscopy after staining protocols and mineral deposition was detected for all groups. Figures 15(a) and (b) shows mineral formation on CHI, CHI-M and CHI-S scaffolds with Alizarin red and von Kossa staining for 28th day incubation period. Stereo images indicated that, mucus and slime extract incorporation induced the phosphate deposition when compared with the control group

CHI. Especially, calcium mineral deposition was observed for all groups due to the calcium carbonate granule content of *H. aspersa* secretions extracts [55]. So, Stereo images showed no distinct difference between extract incorporated groups. Thus, Alizarin Red extraction method was used to determine the difference in calcium deposition between groups. Spectrophotometric results showed that mucus and slime incorporation significantly increased the calcium deposition. On the other hand, among all groups, CHI-M scaffolds had the highest mineralization activity (figure 15(c)). Similarly, Kantawong *et al* investigated the effect of mucus extract of a different species *A. fulica* on biomineralization of dental pulp cells. Results showed that mucus extract induced the mineralized nodule formation of cells compared to control group at 21 d of incubation [48].

#### 4.2.6. COMP content

COMP is a glycoprotein in cartilage tissue that function at cell surfaces and in the extracellular matrix [56]. Besides, COMP plays a part in preserving matrix mechanical properties [57]. COMP content for scaffolds was evaluated with ELISA assay. Since COMP is an early-stage biomarker for chondrocyte bioactivity, measurements were performed on the 3rd and 7th day (figure 16(b)). ELISA results showed



that COMP secretion of SW1353 cells was higher on mucus and slime incorporated scaffolds at 3rd day whereas, COMP secretion levels of SW1353 cells decreased on composite scaffolds at 7th day. The difference in COMP content between groups was not found statistically significant.

#### 4.2.7. Hydroxyproline (HP) content

HP is known as a non-essential amino acid in collagens that exist in skin tissue, and it is found in collagenous fiber in connective tissue [58, 59]. In this study, HP content was determined with sandwich ELISA assay. Spectrophotometric results indicated that HP content of SW1353 cells increased on CHI-M scaffolds at 14th day whereas, no significant increase was observed on mucus and slime incorporated scaffolds on 21st and 28th day when compared with control CHI scaffold. All groups showed similar increasing trend in HP production at the end of the incubation period (figure 16(c)).

#### 4.2.8. GAG content

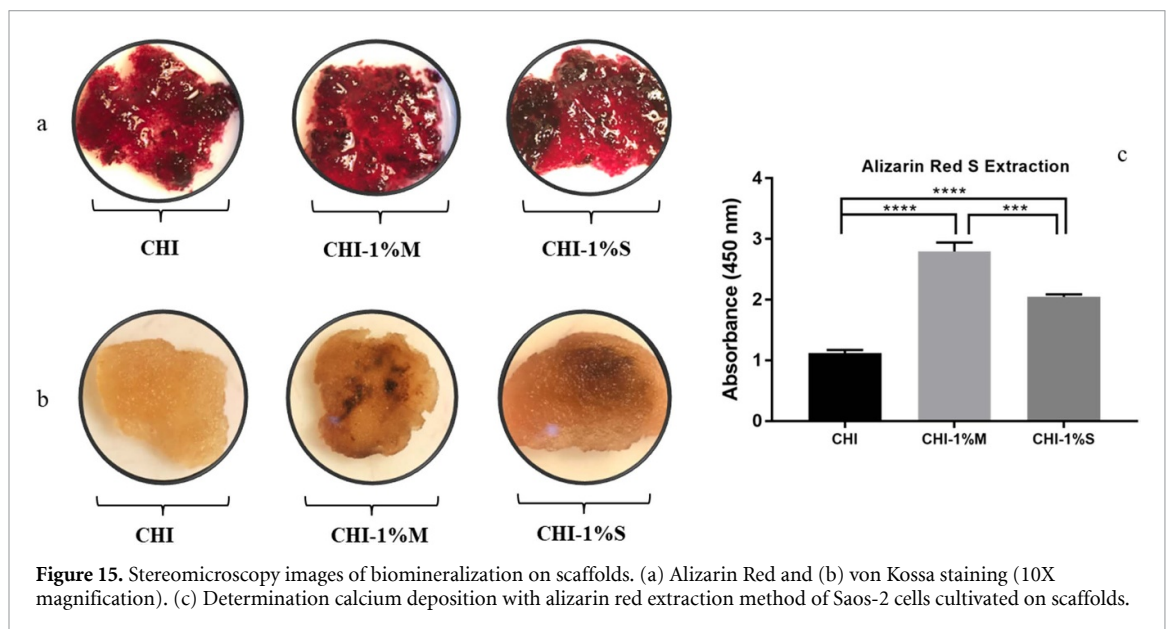
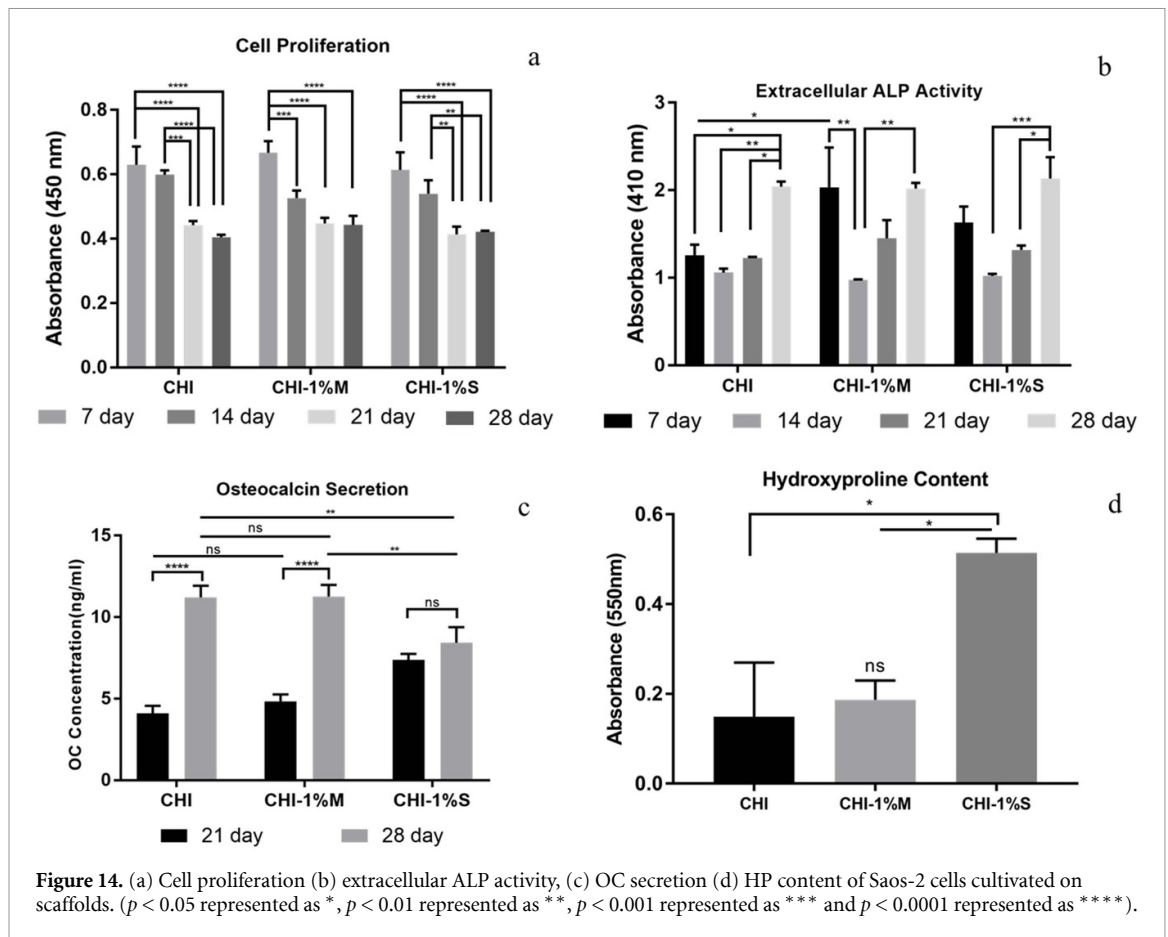
GAGs are long, unbranched polysaccharide chains made up primarily of repeating disaccharide units. GAGs are known as are major components of the tissue extracellular matrix with important physiological functions endow the tissue with resistance to

compressive loading. GAGs are synthesized covalently bound to core proteins to form proteoglycans such as aggrecan with the exception of hyaluronan (HA). GAGs provide the tissue resistance against compressive loading and they are involved in many biological interactions. Chondroitin sulphate (CS), keratan sulphate (KS), and HA are three classes of GAGs found in articular cartilage GAGs and are involved in many biological interactions. CS, KS, and HA are three classes of GAGs found in articular cartilage [60, 61]. GAG secretion of SW1353 cells on CHI-M and CHI-S composite scaffolds were found higher at 14th day of incubation (figure 16(d)). However, GAG content was found higher on CHI group at 21st and 28th day. This may result from possible degradation products of CHI matrix which is composed of sulfated GAGs.

### 4.3. Histological and immunohistochemical staining

#### 4.3.1. Histological staining

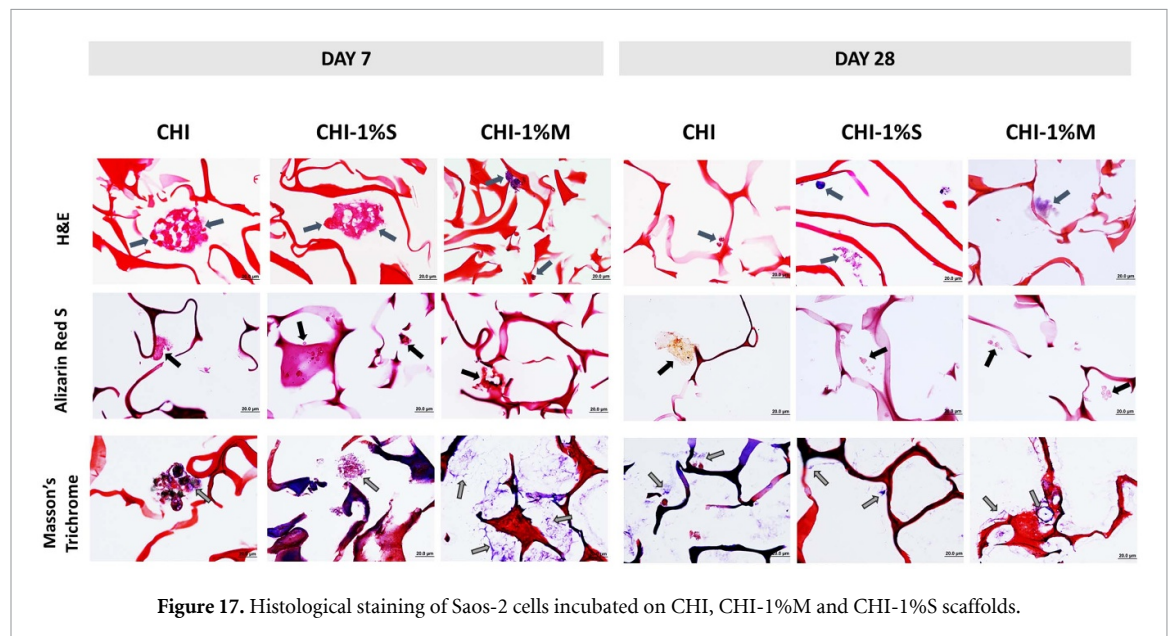
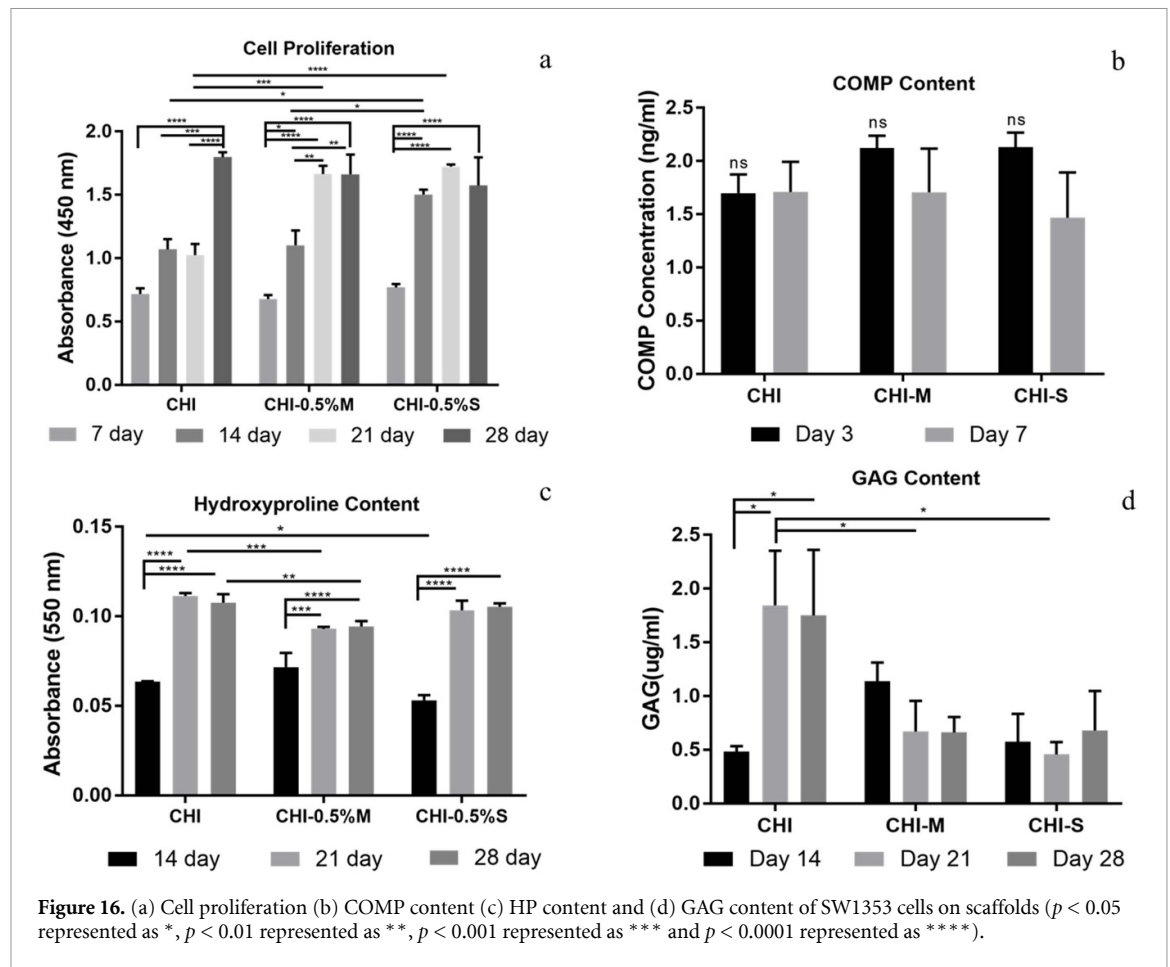
Figures 17 and 18 show the histochemical evaluations of ECM synthesized by Saos-2 and SW1353 cells in mucus and slime incorporated CHI scaffolds respectively. H&E images of Saos-2 cells indicated that CHI and CHI-1%S groups showed differences in



the morphology and distribution of Saos-2 cells on day 7. Spheroid cell colonies were detected around pore walls whereas, Saos-2 cells were observed individually and disorganized in the CHI 1%M scaffold (figure 17). This may arise from the surface adhesiveness of mucus incorporated scaffolds. At the end of 28 d, spheroid structures of the cells were disrupted, and the individual distribution of the cells was detected due to the biomineralization process on scaffold

surface. Alizarin Red S (red/purple) staining images showed inorganic calcium accumulation of Saos-2 cells on scaffolds. Histological images indicated that calcium accumulation was found to be higher than CHI and CHI-S scaffolds at 7th day. In addition, a decrease in inorganic calcium deposition of Saos-2 cells was observed in all groups on 28 d of incubation. Masson Trichrome staining images showed that collagen secretion was observed for all groups.

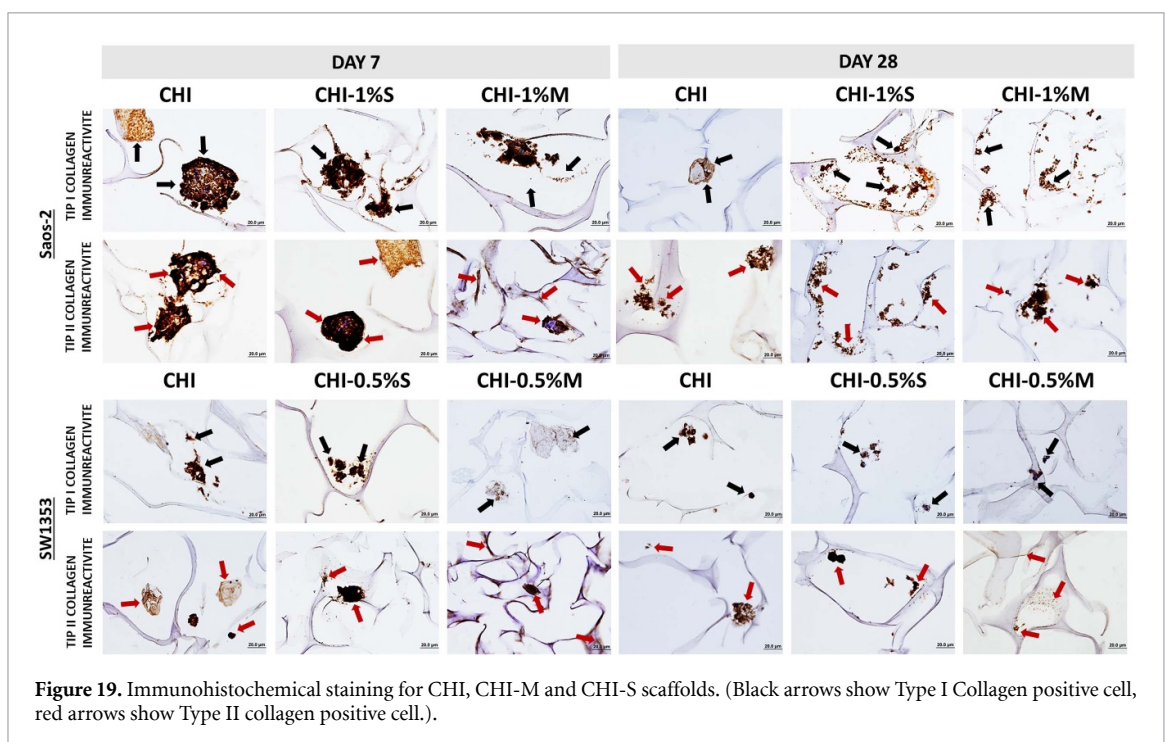
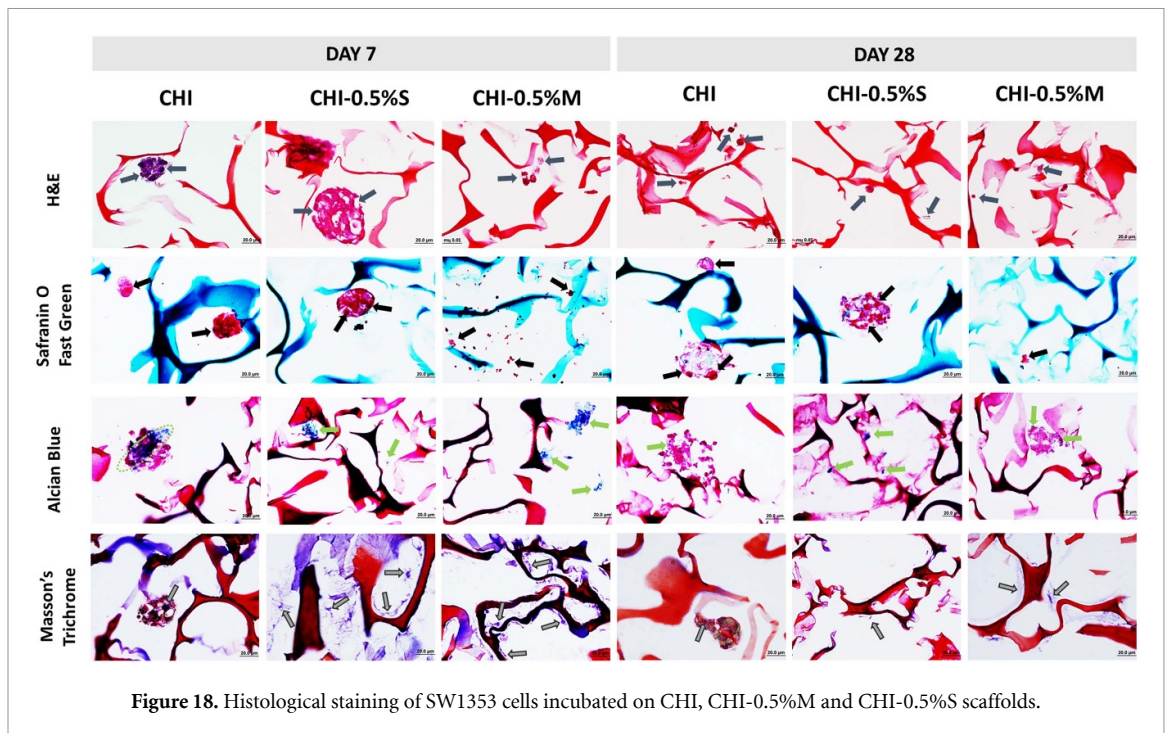




However, collagen production of Saos-2 cells incubated on CHI-M scaffolds was found higher compared to CHI control and CHI-S groups at 7th day.

Figure 18 shows the histochemical evaluations of ECM synthesized by SW1353 cells in CHI, CHI-0.5%S and CHI-0.5%M scaffolds. Morphology and the distribution of SW1353 cells on CHI-S and

CHI-M showed distinct differences as observed on histological images of Saos-2 cells. SW1353 cells colonized in spheroid morphology on CHI-S group. However, cells were distributed as monolayer on CHI-M scaffold. Cartilage tissue is mainly composed of GAG content (15%–25%) which is produced by mature chondrocytes in the extracellular matrix [62].



Thus, GAG detection is identified as an important marker for cartilage regeneration. Alcian Blue and Safranin O staining images indicated that higher amount of GAG components was found in CHI-0.5%S group on 7 and 28 d compared to CHI-0.5%M and CHI groups. Also, GAG production was maintained functionally on 7 and 28 d in the CHI group. Safranin O staining images indicated that pericellular matrix accumulation was observed more in CHI 0.5%S scaffolds at 7th day. At 28 d of incubation,

collagen accumulation was observed to decrease in both CHI-0.5%S and CHI-0.5%M scaffolds compared to 7th day. Consequently, Saos-2 and SW1353 cells on all scaffold groups preserved their morphology and exhibited extracellular matrix formation. Histological images indicated that slime incorporated scaffold groups showed a positive effect on cell proliferation and migration. However, mucus incorporated scaffold groups positively affected the production of extracellular matrix components.

#### 4.3.2. Immunohistochemical staining

Figure 19 shows immunohistochemical evaluations of Type I and Type II collagen synthesized by Saos-2 and SW1353 cells in CHI, CHI-S and CHI-M scaffolds. Histological images indicated that Saos-2 and SW1353 cells showed positive immunoreactivity with regard to the secretion of Type I and Type II collagen at 7 and 28 d of incubation. Saos-2 cells showed higher immunoreactivity intensity compared to SW1353 cells. Type I collagen formation of Saos-2 cells was not found significantly different on 7 d concerning the scaffold groups. SW1353 cells showed higher immunoreactivity on CHI-M and CHI-S scaffolds with regard to the Type II collagen formation. At 7th day, type I and II collagen formation of Saos-2 cells were localized around cell colonies at high levels whereas, at 28th day collagen formation distributed all around the pore walls with decreasing level. However, type I and II formations of SW1353 cells on scaffold groups were observed as localized regions at lower levels. This may result from that Saos-2 cells were incubated with CHI-M and CHI-S at higher extract concentrations. Thus, it can be concluded that high extract concentrations significantly affect Type I and Type II collagen expressions.

## 5. Conclusion

*H. aspersa* snail secretions draw attention as biologically active materials to be used in tissue engineering and biomedical applications. In this study, mucus and slime extracts of *H. aspersa* were successfully loaded in CHI matrix and fabricated via freeze-drying technique. Characterization results indicated that, mucus and slime incorporation enhanced the mechanical properties and increased biodegradation rate of CHI matrix. However, swelling ratio of CHI-M and CHI-S scaffolds decreased due to the decrease in pore size with increasing extract concentration. Highly porous scaffolds were obtained in the range of 81%–90%. The antimicrobial results indicated that mucus and slime extracts and their release solutions showed antimicrobial effect on *S. epidermidis* and *P. Fluorescens*. *In vitro* bioactivity results indicated that mucus and slime incorporation enhanced the osteogenic activity by inducing ALP activity, OC secretion and calcium deposition for biomineralization. In addition, CHI-M and CHI-S composite scaffolds induced GAG secretion of SW1353 cells and induced chondrogenic activity. Immunohistochemical staining images showed that Type I and Type II collagen expressions significantly increased at extract loaded scaffolds with higher concentrations. In conclusion, *H. aspersa* snail secretions are composed of bioactive components show potential as bioactive reinforcements with their osteogenic and chondrogenic bioactivity for both bone and cartilage tissue regeneration as well as enhanced physical properties.

## Data availability statement

All data that support the findings of this study are included within the article (and any supplementary files).

## Acknowledgments

The authors thank Assistant Professor Dr Meltem Alper from Aksaray University for supplying Saos-2 cell line. The authors thank Professor Dr Figen Korel from Izmir Institute of Technology for supplying *Pseudomonas fluorescens* strain. The authors are grateful to Izmir Institute of Technology (Iztech) Biotechnology and Bioengineering Research and Application Center (IZTECH BIOMER) for antimicrobial tests, FT-IR analysis and fluorescence microscopy, Center for Material Research (IZTECH CMR) for SEM analysis. This research did not receive any specific grant from funding agencies in the public, commercial, or not-for-profit sectors.

## ORCID iD

Funda Tihminlioglu  <https://orcid.org/0000-0002-3715-8253>

## References

- [1] Temenoff J S and Mikos A G 2000 Review: tissue engineering for regeneration of articular cartilage *Biomaterials* **21** 431–4
- [2] O'driscoll S 1998 The healing and regeneration of articular cartilage *J. Bone Joint Surg. Am.* **80** 1795–812
- [3] Awad H A, O'Keefe R J, Lee C H and Mao J J 2014 Bone tissue engineering: clinical challenges and emergent advances in orthopedic and craniofacial surgery *Principle of Tissue Engineering* 4th edn, ed R Lanza, R Langer and J Vacanti (Boston: Academic Press Inc) pp 1733–43
- [4] Li W J, Laurencin C T, Catterson E J, Tuan R S and Ko F K 2002 Electrospun nanofibrous structure: a novel scaffold for tissue engineering *J. Biomed. Mater. Res.* **60** 613–21
- [5] Dolcimascolo A, Calabrese G, Conoci S and Parenti R 2019 Innovative biomaterials for tissue engineering *Biomaterial-supported Tissue Reconstruction or Regeneration* ed M Barbeck, O Jung, R Smeets and T Korzinskas (London: IntechOpen) pp 1–18
- [6] Ha T L B, Quan T M, Vu D N and Si D M 2013 Naturally derived biomaterials: preparation and application *Regenerative Medicine and Tissue Engineering* ed J A Andrades (London: IntechOpen) pp 247–69
- [7] Tamburaci S, Kimna C and Tihminlioglu F 2018 Novel phytochemical *Cissus quadrangularis* extract-loaded chitosan/Na-carboxymethyl cellulose-based scaffolds for bone regeneration *J. Bioact. Compat. Polym.* **33** 1–18
- [8] Singh P, Gupta A, Qayoom I, Singh S and Kumar A 2020 Orthobiologics with phytoactive cues: a paradigm in bone regeneration *Biomed. Pharmacother.* **130** 110754
- [9] Irgin C, Çörekçi B and Ozan F 2016 Does stinging nettle (*Urtica dioica*) have an effect on bone formation in the expanded inter-premaxillary suture? *Arch. Oral Biol.* **69** 13–18
- [10] Hadavi M et al 2017 Novel calcified gum Arabic porous nano-composite scaffold for bone tissue regeneration *Biochem. Biophys. Res. Commun.* **488** 671–8
- [11] Brieva A et al 2008 Molecular basis for the regenerative properties of a secretion of the mollusk *Cryptomphalus aspersa* *Skin Pharmacol. Physiol.* **21** 15–22

- [12] Trapella C et al 2018 HelixComplex snail mucus exhibits pro-survival, proliferative and pro-migration effects on mammalian fibroblasts *Sci. Rep.* **8** 17665 1–10
- [13] Tsoutsos D, Kakagia D and Tamparopoulos K 2009 The efficacy of *Helix aspersa* Müller extract in the healing of partial thickness burns: a novel treatment for open burn management protocols *J. Dermatolog. Treat.* **20** 219–22
- [14] Otsuka-Fuchino H et al 1992 Bactericidal action of a glycoprotein from the body surface mucus of giant African snail *Camp. Biochem. Physiol.* **101** 607–13
- [15] Etim L B, Aleruchi C and Attah O G 2016 Antibacterial properties of snail mucus on bacteria isolated from patients with wound infection *Br. Microbiol. Res. J.* **11** 1–9
- [16] Pitt S J, Graham M A, Dedi C G, Taylor-Harris P M and Gunn A 2015 Antimicrobial properties of mucus from the brown garden snail *Helix aspersa* *Br. J. Biomed. Sci.* **72** 174–81
- [17] Ng T P T et al 2013 Snails and their trails: the multiple functions of trail-following in gastropods *Biol. Rev. Camb. Phil. Soc.* **88** 683–700
- [18] Greistorfer S et al 2017 Snail mucus—glandular origin and composition in *Helix pomatia* *Zoology* **122** 126–38
- [19] Angulo D E L and Sobral P J A 2016 Characterization of gelatin/chitosan scaffold blended with aloe vera and snail mucus for biomedical purpose *Int. J. Biol. Macromol.* **92** 645–53
- [20] di Filippo M F et al 2020 Functional properties of chitosan films modified by snail mucus extract *Int. J. Biol. Macromol.* **143** 126–35
- [21] Freier T, Koh H S, Kazazian K and Shoichet M S 2005 Controlling cell adhesion and degradation of chitosan films by N-acetylation *Biomaterials* **26** 5872–8
- [22] Hoemann C D, El-Gabalawy H and McKee M D 2009 *In vitro* osteogenesis assays: influence of the primary cell source on alkaline phosphatase activity and mineralization *Patho. Biol.* **57** 318–23
- [23] Li Z et al 2020 Biomechanically, structurally and functionally meticulously tailored polycaprolactone/silk fibroin scaffold for meniscus regeneration *Theranostics* **10** 5090–106
- [24] Kim Y T et al 2012 The dynamic healing profile of human periodontal ligament stem cells: histological and immunohistochemical analysis using an ectopic transplantation model *J. Periodontal. Res.* **47** 514–24
- [25] Brauker J H et al 1995 Neovascularization of synthetic membranes directed by membrane micro architecture *J. Biomed. Mater. Res.* **29** 1517–24
- [26] Klawitter J J and Hulbert S F 1971 application of porous ceramics for the attachment of load-bearing internal orthopedic applications *J. Biomed. Mater. Res.* **2** 161–8
- [27] Yang S, Leong K F, Du Z and Chua C K 2001 The design of scaffolds for use in tissue engineering part 1: traditional factors *Tissue Eng.* **7** 679–89
- [28] Whang K et al 1999 Engineering bone regeneration with bioabsorbable scaffolds with novel microarchitecture *Tissue Eng.* **5** 35–51
- [29] Yannas I V, Lee E, Orgill D P and Skrabut E M 1989 Synthesis and characterization of a model extracellular matrix that induces partial regeneration of adult mammalian skin *Proc. Natl Acad. Sci.* **86** 933–7
- [30] Zhang Q, Lu H, Kawazoe N and Chen G 2014 Pore size effect of collagen scaffolds on cartilage regeneration *Acta Biomater.* **10** 2005–13
- [31] Kramschuster A and Turng L S 2013 Fabrication of tissue engineering scaffolds *Handbook of Biopolymers and Biodegradable Plastics* ed S Ebnesajjad (UK: Elsevier Inc.) pp 427–46
- [32] Xie J et al 2006 Mechano-active scaffold design based on microporous poly(L-lactide-co-epsilon-caprolactone) for articular cartilage tissue engineering: dependence of porosity on compression force-applied mechanical behaviors *Tissue Eng.* **12** 449–58
- [33] Cheng A et al 2019 Advances in porous scaffold design for bone and cartilage tissue engineering and regeneration *Tissue Eng. B* **25** 14–29
- [34] Vishwanath V, Pramanik K and Biswas A 2016 Optimization and evaluation of silk fibroin-chitosan freeze-dried porous scaffolds for cartilage tissue engineering application *J. Biomater. Sci., Polym. Ed.* **27** 657–74
- [35] Pawlicki J M et al 2004 The effect of molluscan glue proteins on gel mechanics *J. Exp. Biol.* **207** 1127–35
- [36] Leceta I, Guerrero P and de la Caba K 2013 Functional properties of chitosan-based films *Carbohydr. Polym.* **93** 339–46
- [37] Ibrahim M, Mahmoud A A, Osman O, Refaat A and El-Sayed E S M 2010 Molecular spectroscopic analysis of nano-chitosan blend as biosensor *Spectrochim. Acta. A* **77** 802–6
- [38] Dona T M, Kingb C F, Chiub W Y and Peng C A 2006 Preparation and characterization of chitosan-g-poly(vinyl alcohol)/poly(vinyl alcohol) blends used for the evaluation of blood-contacting compatibility *Carbohydr. Polym.* **63** 331–9
- [39] Skingsley D R, White A J and Weston A 2000 Analysis of pulmonate mucus by infrared spectroscopy *J. Moll. Stud.* **66** 363–71
- [40] Pancake S J and Karnovsky M L 1971 The isolation and characterization of a mucopolysaccharide secreted by the snail, *Otella lactea* *J. Biol. Chem.* **264** 253–62
- [41] Fathi M, Nasrabadi M N and Varshosaz J 2017 Characteristics of vitamin E-loaded nanofibres from dextran *Int. J. Food Prop.* **20** 2665–74
- [42] Tallian C et al 2019 Lysozyme-responsive spray-dried chitosan particles for early detection of wound infection *ACS Appl. Bio. Mater.* **2** 1331–9
- [43] Hutmacher D W, Goh J C H and Teoh S H 2001 An introduction to biodegradable materials for tissue engineering applications *Ann. Acad. Med. Singap.* **30** 183–91 PMID: 11379417
- [44] Cheung H Y, Lau K T, Lu T P and Hui D 2007 A critical review on polymer-based bio-engineered materials for scaffold development *Composites B* **38** 291–300
- [45] Dolashka P et al 2015 Bioactive compounds isolated from garden snails *J. BioSci. Biotechnol.* 147–55
- [46] Gill S R et al 2005 Insights on evolution of virulence and resistance from the complete genome analysis of an early methicillin-resistant *Staphylococcus aureus* strain and a biofilm-producing methicillin-resistant *Staphylococcus epidermidis* strain *J. Appl. Bacteriol.* **187** 2426–38
- [47] Scales B S, Dickson R P, LiPuma J J and Huffnagle G B 2014 Microbiology, genomics, and clinical significance of the *Pseudomonas fluorescens* species complex, an unappreciated colonizer of humans *Clin. Microbiol. Rev.* **27** 927–48
- [48] Kantawong F et al 2016 Mucus of *Achatina fulica* stimulates mineralization and inflammatory response in dental pulp cells *Turk. J. Biol.* **40** 353–9
- [49] Angulo D E et al 2019 Fabrication, characterization and *in vitro* cell study of gelatin-chitosan scaffolds: new perspectives of use of aloe vera and snail mucus for soft tissue engineering *Mater. Chem. Phys.* **234** 268–80
- [50] Anselme K 2000 Osteoblast adhesion on biomaterials *Biomaterials* **21** 667–81
- [51] Golub E E and Battaglia K B 2007 The role of alkaline phosphatase in mineralization *Curr. Opin. Orthop.* **18** 444–8
- [52] Hauschka P V, Lian J B and Gallop P M 1975 Direct identification of the calcium-binding amino acid, gamma-carboxyglutamate, in mineralized tissue *Proc. Natl Acad. Sci. USA* **72** 3925–9
- [53] Ignat'eva N Y, Danilov N A, Averkiev S V, Obrezkova M V and Lunin V V 2007 Determination of hydroxyproline in tissues and the evaluation of the collagen content of the tissues *J. Anal. Chem.* **62** 51–57
- [54] Bilgen G, Oktay G, Tokgöz Z, Güner G and Yalçın S 1999 Collagen content and electrophoretic analysis of type I collagen in breast skin of heterozygous naked neck and normally feathered commercial broilers *Turk. J. Vet. Anim. Sci.* **23** 483–8

- [55] Fournie J and Chetail M 1984 Calcium dynamics in land gastropods *Am. Zool.* **24** 857–70
- [56] McKee M D and Cole W G 2012 Bone matrix and mineralization *Pediatric Bone* 2nd edn, ed F H Glorieux, J M Pettifor and H Jüppner (San Diego: Academic Press Inc.) pp 9–37
- [57] Caldeira J, Sousa A, Sousa D M and Barros D 2018 Extracellular matrix constitution and function for tissue regeneration and repair *Peptides and Proteins as Biomaterials for Tissue Regeneration and Repair* ed M A Barbosa and M C L Martins (UK:Woodhead Publishing Inc.) pp 29–72
- [58] Weinmann H and Ottow E 2007 Recent development in novel anticancer therapies *Comprehensive Medicinal Chemistry II* ed J B Taylor and D J Triggle (Amsterdam, Netherlands: Elsevier Science Inc.) pp 221–51
- [59] Nakatani S, Mano H, Sampei C, Shimizu J and Wada M 2009 Chondroprotective effect of the bioactive peptide prolyl-hydroxyproline in mouse articular cartilage *in vitro* and *in vivo* *Osteoarthr. Cartil.* **17** 1620–7
- [60] Sharma A, Wood L D, Richardson J B, Roberts S and Kuiper N J 2007 Glycosaminoglycan profiles of repair tissue formed following autologous chondrocyte implantation differ from control cartilage *Arthritis Res. Ther.* **9** R79
- [61] Sodhi H and Panitch A 2020 Glycosaminoglycans in tissue engineering: a review *Biomolecules* **11** 29
- [62] Hu J C Y and Athanasiou K A 2003 Structure and function of articular cartilage *Handbook of Histology Methods for Bone and Cartilage* ed Y H An and K L Martin (Totowa NJ: Humana Press Inc.) pp 73–95